Explainable machine learning for predicting compressive strength of rubberized concrete SHAP interpretation, lifecycle assessment, and design recommendations

Tan, Xiao; Xing, Jianglei; Wang, Yuan; Qiu, Haotian; Mahjoubi, Soroush; Guo, Pengwei

DOI
10.1016/j.jclepro.2025.147338

Licence
CC BY

Publication date
2025

Document Version
Final published version

Published in
Journal of Cleaner Production

Citation (APA)
Tan, X., Xing, J., Wang, Y., Qiu, H., Mahjoubi, S., & Guo, P. (2025). Explainable machine learning for predicting compressive strength of rubberized concrete: SHAP interpretation, lifecycle assessment, and design recommendations. *Journal of Cleaner Production*, *538*, Article 147338. https://doi.org/10.1016/j.jclepro.2025.147338

Journal of Cleaner Production 538 (2026) 147338

Contents lists available at ScienceDirect

Journal of Cleaner Production

journal homepage: www.elsevier.com/locate/jclepro

Explainable machine learning for predicting compressive strength of rubberized concrete: SHAP interpretation, lifecycle assessment, and design recommendations

Xiao Tan [a,b,*], Jianglei Xing [a], Yuan Wang [a,b], Haotian Qiu [a], Soroush Mahjoubi [c], Pengwei Guo [d,**]

[a] College of Water Conservancy and Hydropower Engineering, Hohai University, Nanjing, Jiangsu, 210024, China
[b] The National Key Laboratory of Water Disaster Prevention, Nanjing, Jiangsu, 210024, China
[c] Department of Civil and Environmental Engineering, Massachusetts Institute of Technology, Cambridge, MA, 02139, United States
[d] Faculty of Civil Engineering and Geosciences, Delft University of Technology, Delft, 2628 CN, Netherlands

ARTICLE INFO

Keywords:
Rubberized concrete
Machine learning
SHAP analysis
Compressive strength
Life cycle assessment

ABSTRACT

The study explores dataset preparation, machine learning (ML) model training, interpretation, and life cycle assessment (LCA) to predict and enhance the performance and sustainability of rubberized concrete. A large dataset comprising 1209 collected samples with nine input features was used to train and evaluate six machine learning models. Among the six models, the Light gradient boosting machine (LightGBM) model achieved the highest prediction accuracy on the testing dataset, with an R^2 value exceeding 0.96, a MAPE of 8.31 %, a MAE of 2.36 MPa, and a RMSE of 3.25 MPa. The SHAP algorithm was used to interpret predictions and identify key factors influencing compressive strength. Rubber content and water-to-cement ratio reduced strength, while longer curing time, more superplasticizer, higher fine aggregate content, and a greater silica fume-to-cement ratio improved it. Coarse aggregate, crumb rubber size, and cement content had minimal impact. Optimal performance was achieved with: Rubber content <55.92 kg/m^3, w/c ratio <0.4, curing time >26 days, superplasticizer >3.7 kg/m^3, fine aggregate >642 kg/m^3, and silica fume/cement ratio >2.5 %. LCA results show that, although rubberized concrete offers no clear advantage over conventional concrete in cost, carbon, or energy, the lower strength and higher superplasticizer use of rubberized concrete lead to greater strength-normalized impacts, and therefore its value lies more in waste recycling and toughness than in strength-based sustainability. The unique advantage of this research lies in the development of a ML-LCA integration framework that synthetically balances performance prediction and sustainability assessment of rubberized concrete, with delivering actionable mix design recommendations, identifying key and low-impact variables, and revealing trade-offs among strength, cost, and environmental performance.

Abbreviation List

Abbreviation	Full name
ANN	Artificial neural network
CART	Classification and Regression Tree
C_C	Content of cement
C_{CA}	Content of coarse aggregate
C_{FA}	Content of fine aggregate
C_R	Content of rubber
C_S	Content of superplasticizer
ERT	Extremely randomized trees
f_c	Compressive strength
GBDT	Gradient Boosting Decision Tree
LCA	Life cycle assessment
LightGBM	Light gradient boosting machine
LOWESS	Locally Weighted Scatterplot Smoothing

(*continued on next column*)

(*continued*)

(*continued on next page*)

* Corresponding author. College of Water Conservancy and Hydropower Engineering, Hohai University, Nanjing, Jiangsu, 210098, China.
** Corresponding author.
E-mail addresses: xiaotan@hhu.edu.cn (X. Tan), p.guo-1@tudelft.nl (P. Guo).

https://doi.org/10.1016/j.jclepro.2025.147338
Received 28 May 2025; Received in revised form 24 October 2025; Accepted 13 December 2025
Available online 22 December 2025

(*continued*)

Abbreviation	Full name
MAE	Mean absolute error
MAPE	Mean absolute percentage error
ML	Machine learning
ML-LCA	Machine learning-Life cycle assessment
R^2	Coefficient of determination
RBF	Radial Basis Function
RF	Random forest
RMSE	Root mean square error
SCMs	Supplementary cementitious materials
sf/c	Ratio of silica fume to cement
SHAP	SHapley Additive exPlanations
S_R	Maximum size of crumb rubber
SVM	Support vector machines
T_C	Curing time
w/c	Water-to-cement ratio
XGBoost	Extreme gradient boosting trees

1. Introduction

Concrete is widely used in construction due to its high compressive strength and long-term durability (Khan and McNally, 2023). The material can be easily molded into various shapes and works well with steel reinforcement, making it highly versatile for structural applications in buildings, bridges, pavements, and other infrastructure. Its popularity in infrastructure and construction projects is also driven by broad availability and low production costs. However, despite these advantages, conventional concrete remains brittle, with low impact resistance and limited energy absorption, making it vulnerable to cracking under dynamic or impact loads (Maurya et al., 2023; Zhou et al., 2023).

To overcome these challenges, researchers have proposed using rubber particles as an alternative to traditional aggregates in concrete (Zhu and Jiang, 2023). This approach has led to the development of rubberized concrete, which offers improved toughness, enhanced impact resistance, and increased durability compared to conventional mixtures (Dissanayake et al., 2021; Surehali et al., 2023). Experimental investigations have revealed that columns made of rubberized concrete demonstrate superior energy dissipation capabilities when subjected to cyclic loading (Moustafa et al., 2017). Their deformation and rotational capacity can be up to 50 % higher than that of conventional concrete columns (Pham et al., 2018). Moreover, rubberized concrete bridge columns improve safety in vehicle collisions by absorbing more impact energy and reducing the force transferred to the vehicle (Lavagna et al., 2020). The rapid growth of the automotive industry has led to increased tire production, resulting in a significant accumulation of waste rubber. Rubber is a non-degradable material that resists decomposition in water or organic solvents, allowing it persist in landfills for centuries and create serious environmental risks (Karunarathna et al., 2022). The utilization of rubber waste in concrete offers a practical solution to mitigate this environmental burden.

Although rubberized concrete has demonstrated promising performance in various studies, its widespread adoption is limited by the significant reduction in compressive strength caused by the inclusion of waste rubber (Lavagna et al., 2020; El-Gammal et al., 2010). Research indicates that substituting 50 % of sand and gravel with ground rubber and tire chips can reduce the compressive strength by up to 85 %, leaving only 15 % of the original strength (Güneyisi et al., 2004). Other investigations have reported similar strength losses due to the addition of waste rubber in concrete (Mohammed and Azmi, 2014; Liu et al., 2020). To quantify the influence of rubber on compressive strength, empirical models have been proposed using experimental data where fine aggregates were partially replaced with crumb rubber (Mohammed and Azmi, 2014). Although the model achieved a high fitting accuracy ($R^2 = 0.97$), its generalization capability is constrained by two main limitations: The applicability of the model is limited using slump-based piecewise functions and the focus on fine aggregate replacement with rubber particles.

Recent studies have shown growing interest in applying ML to the design of rubberized concrete mixtures (Jaf et al., 2024). ML is valued for its strong predictive capabilities and ability to capture the complex behavior of composite materials. Unlike conventional empirical methods, ML models can process large and diverse datasets to identify hidden patterns and interactions among mix components that affect compressive strength (Xie et al., 2020; Guo et al., 2024; Zhou et al., 2024; Ly et al., 2021). A variety of algorithms, including deep neural networks (Gregori et al., 2021), Gaussian process modeling (Kovačević et al., 2021), Random Forest (Zhou and Zheng, 2025), and networks enhanced by genetic algorithm (Zhang et al., 2021), have been used to accurately predict the mechanical properties of rubberized concrete. For example, ensemble models have predicted the compressive strength of rubberized concrete with a Pearson correlation above 0.96 (Kovačević et al., 2021), while ANN and XGBoost achieved R^2 values over 0.98 (Zhou and Zheng, 2025). Various ML models have also been applied to self-compacting rubberized concrete, reaching an R^2 over 0.94 (Zrar et al., 2024). Four predictive models were employed to forecast the compressive strength of self-compacting rubberized concrete, achieving an R^2 of 0.94 (Sherwani et al., 2025). These approaches consistently outperform traditional empirical formulas, demonstrating strong generalization and adaptability across diverse mixture designs.

Despite these advancements, challenges remain in applying data-driven predictive models to forecast the compressive strength of rubberized concrete: (1) Most existing studies rely on relatively small datasets, often limited to a few hundred samples (Kovačević et al., 2021; Zhou and Zheng, 2025; Zhang et al., 2021). This restricts the ability of models to generalize well across diverse mix designs and environmental conditions, potentially leading to overfitting and unreliable predictions when applied to new cases. (2) Many machine learning models lack transparency, making it challenging for engineers to understand the influence of mix design parameters on compressive strength. (3) While predicting strength is important, sustainability remains a critical aspect that must also be addressed. Most current research lacks integration of LCA into machine learning workflows, limiting the ability to fully evaluate the sustainability and cost impacts of rubberized concrete formulations.

To achieve a systematic assessment between mechanical and sustainable performance, this research tackles the identified challenges by establishing a ML-LCA integration framework. This framework leverages a large-scale dataset to develop robust and interpretable machine learning models for predicting the compressive strength of rubberized concrete. Meanwhile, by incorporating LCA into the predictive process, the framework enables both accurate performance forecasting and informed decision-making for sustainable mix design. It addresses key gaps in existing studies, such as limited sample sizes, poor model transparency, and the lack of sustainability considerations.

The key novelties of this research can be summarized as follows: (1) A unique ML-LCA integration framework is developed that synthetically integrates strength prediction with sustainability evaluation, which providing a holistic balance between mechanical performance and eco-efficiency, enabling sustainability comparisons, and supporting informed recommendations for rubberized concrete use. (2) Development of the largest dataset (1209 samples) on rubberized concrete compressive strength and integration of SHapley Additive exPlanations (SHAP) analysis to quantify the influence of each design parameter. The full dataset is used for detailed parametric analysis, providing new insights into both magnitude and direction of each variable influence.

2. Methodology

Fig. 1 presents the developed framework in this study, including four main steps.

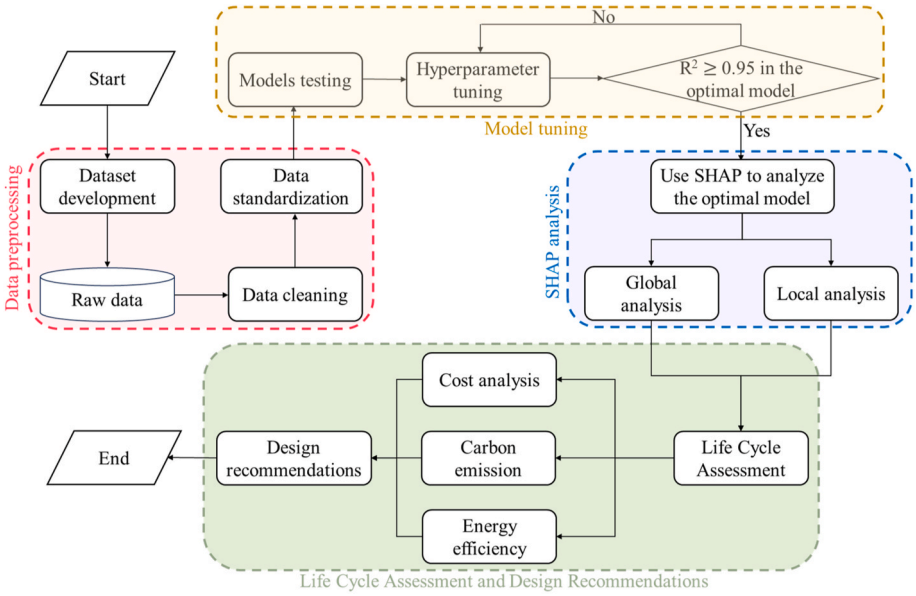

Fig. 1. The flowchart of proposed multi-model prediction, SHAP analysis and life cycle assessment.

(1) Dataset preparation. The dataset was compiled from rubberized concrete literature and uses mixture design parameters as inputs with compressive strength as the output. Data cleaning and normalization were performed to ensure consistency and enhance the overall quality of the dataset.
(2) Predictive modeling. Several ML models were trained and tuned to improve performance. The algorithm with the highest prediction accuracy was selected to estimate the compressive strength of rubberized concrete.
(3) Model explanation. SHAP analysis was used to interpret the optimal model, providing global insights and feature-level importance for the input variables.
(4) Life cycle assessment. LCA at the mixture design stage evaluated the cost, carbon footprint, and energy efficiency of rubberized concrete production. Compressive strength was used to normalize cost, carbon footprint, and energy use, enabling strength-adjusted sustainability metrics. Design recommendations were proposed to identify the most resource-efficient strategies for rubberized concrete development.

2.1. Dataset description and preprocessing

2.1.1. Dataset preparation

A comprehensive database of 1209 rubberized concrete mixtures was compiled from diverse sources for predicting compressive strength, as detailed in the Supplementary Data. The database was collected from 62 articles published between 2004 and 2024 (Güneyisi et al., 2004; Mohammed and Azmi, 2014; Liu et al., 2020; Abdullah et al., 2024; Agrawal et al., 2023, 2024; Aiello and Leuzzi, 2010; Aliabdo et al., 2015; Alizadeh et al., 2024; Beiram and Al-Mutairee, 2022; Bignozzi and Sandrolini, 2006; Bing and Ning, 2014; Bulut, 2024; Choudhary et al., 2020; Dai et al., 2013; Elbialy et al., 2024; Fadiel et al., 2023a,b; Faraj et al., 2019; Fernández-Ruiz et al., 2018; Gesoglu et al., 2015; Gesoğlu and Güneyisi, 2007; Güneyisi, 2010; Gupta et al., 2016, 2021a,b; Jalal et al., 2019; Kechkar et al., 2020; Kelechi et al., 2022; Khern et al., 2020; Kumar et al., 2023; Li et al., 2016a; Liu et al., 2013, 2016; Luong et al., 2017; Lv et al., 2019; Ma and Yue, 2013; Medina et al., 2016; Mehdipour et al., 2020; Mishra and Panda, 2015; Mohd Nasir et al., 2022; Moolchandani et al., 2024; Noaman et al., 2017; Pham et al., 2019; Rahat Dahmardeh et al., 2021; Rezaifar et al., 2016; Safan et al., 2017; Saini et al., 2024; Sanjaya et al., 2023; Sharma et al., 2024; Singh et al., 2022; Skripkiūnas et al., 2009; Strukar et al., 2018; Thomas et al., 2014; Thomas and Gupta, 2016a; Topçu and Bilir, 2009; Yasser et al., 2023; Záleská et al., 2019; Zhang et al., 2014; Zhang and Poon, 2018; Zinkaah et al., 2024). In these studies, the compressive strength for rubberized concrete was obtained through experiments on various samples sizes under standard curing condition. The compressive strength was then standardized to that of a 150 mm^3 cubic specimen to eliminate dimensional differences according to reference (Mansur and Islam, 2002):

$$f_{cu,150} = 0.91 f_{cu,100} + 3.62 \quad (1)$$

where $f_{cu,150}$ and $f_{cu,100}$ represent the compressive strengths of 150 mm^3 and 100 mm^3 cubic specimens, respectively.

Nine variables associated with the mixture design and curing period of rubberized concrete were analyzed to evaluate their impact on compressive strength using ML. These included water-to-cement ratio, cement content, silica fume content, rubber content, fine and coarse aggregate content, maximum crumb rubber size, superplasticizer content, and curing days. The rubber content was calculated based on rubber density, rubber to aggregate volume ratio, and aggregate mass and density, as documented in (Güneyisi et al., 2004). The nine input variables were chosen based on their widely recognized influence on the mechanical performance of rubberized concrete, as evidenced in prior literature. Specifically, parameters such as the water-to-cement ratio, cement, silica fume, aggregate, and superplasticizer contents are fundamental to concrete mix design and significantly affect strength development (Liu et al., 2020; Jaf et al., 2024). Rubber content and maximum rubber size directly influence the mechanical and durability performance of rubberized concrete (Güneyisi et al., 2004). Lastly, curing days are critical in reflecting the hydration progress and strength gain over time. Table 1 shows the minimum, maximum, quartile values, mean, and standard deviation for each input variable along with the compressive strength. Fig. A1 (see Appendix) displays probability density distributions for nine input variables and a single output variable. The compressive strength ranges from 0 to 87 MPa and follows an approximately normal distribution with no evident skewness.

To assess potential multicollinearity and relationships among variables, a Pearson correlation coefficient analysis was performed, as shown in Fig. 2. The analysis indicates that most input features have relatively low intercorrelations ($|R|<0.7$), suggesting weak linear dependence (Guo et al., 2024). This indicates that the selected variables

Table 1
Variation in the input characteristics and compressive strength of rubberized concrete.

Symbol	Unit	Min	Q1	Q2	Q3	Max	Mean	STD
w/c	/	0.3	0.38	0.42	0.5	0.68	0.44	0.09
C_R	kg/m^3	0	16.8	47.5	88.94	490.3	66.38	70.65
S_R	mm	0	1.18	4	5	20	4.35	4.29
C_C	kg/m^3	270	364	400	450	629.27	414.87	63.49
C_{FA}	kg/m^3	0	573	676.1	725.31	1395	649.7	151.09
C_{CA}	kg/m^3	0	848	1024	1124.4	1520	988.32	216.75
Sf/c	%	0	0	0	6	20	2.88	5.02
C_S	kg/m^3	0	0	2.39	5.1	60.45	5.04	9.18
T_C	day	3	28	28	28	365	39.62	44.12
f_c	MPa	1.58	22.93	33.63	44.26	87.46	34.6	15.88

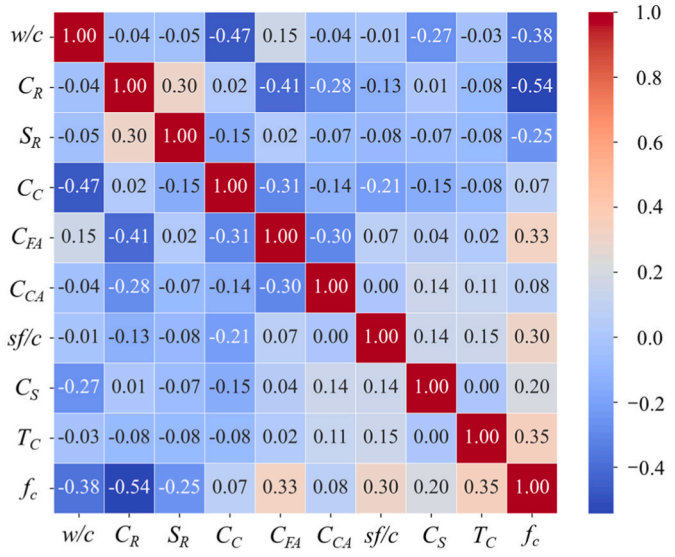

Fig. 2. Heatmap of Pearson correlation coefficient.

are suitable for training ML models, as high intercorrelation can negatively affect model performance and interpretability. Based on these results, all mixture design variables were included as input variables (Zhou et al., 2024).

2.1.2. Data normalization and splitting

The process of data normalization represents a critical procedure in ML workflows, facilitating the adjustment of diverse-scale variables to a uniform scale. This process aids faster convergence by preventing variables on larger scales from dominating the algorithm (Singh and Singh, 2020). Common data standardization techniques include Z-Score Standardization, Min-Max Scaling, Decimal Scaling, and Maximum-Absolute Scaling (Jain et al., 2005). Within the context of this investigation, the input parameters underwent standardization via the Maximum-Absolute technique, adjusting values within a 0 to 1 interval. This approach modifies data points through division by the highest absolute value present in their corresponding feature (Guo et al., 2024). The standardized dataset was shuffled with a fixed random seed to avoid order bias and ensure that the training and testing subsets were representative of the overall data distribution (Zhou et al., 2024). The dataset was subsequently divided, allocating 80 % for training purposes and reserving 20 % for testing (Ejaz et al., 2024).

2.2. Machine learning algorithms

This study employs six machine learning models: ANN, SVM, RF, ERT, XGBoost, and LightGBM. The selection of models was guided by their demonstrated success in predicting concrete strength, as well as their representation of diverse algorithmic paradigms and varying levels of model complexity (Ahmad et al., 2021; Zhang et al., 2024; Paruthi et al., 2022; Guo et al., 2021; Guo et al., 2025). ANN and SVM were selected as classical models with distinct learning strategies, namely neural networks and kernel-based methods, serving as baselines. RF and ERT were included for their robustness and interpretability as ensemble tree-based models. XGBoost and LightGBM, as advanced gradient boosting algorithms, were chosen for their high accuracy and efficiency in processing structured engineering data. The model that achieves the highest prediction accuracy based on R^2, RMSE, and MAE will be selected for subsequent LCA analysis. The details of the machine learning models are summarized below and Table 2.

ANNs are inspired by the human brain using interconnected neuron layers and activation functions (e.g., sigmoid, ReLU) to map inputs to outputs (Kaveh, 2024). They adjust weights and biases via gradient descent to minimize error and typically require large datasets (Apicella et al., 2021; Gardner, 1984). In this study, mixture design variables form the input layer, compressive strength is the output layer, and the network learns the relationship through iterative backpropagation. SVM finds an optimal hyperplane to separate data (Cortes and Vapnik, 1995) and in regression fits a function within a defined error margin (ε) (Lee et al., 2023). Kernel functions (linear, polynomial, RBF, sigmoid) enable adaptation to high-dimensional spaces without altering inputs (Ngu et al., 2024). The ε-insensitive loss ignores errors within the margin and penalizes only larger deviations to improve noise tolerance and generalization. RF is an ensemble method that builds multiple CART regression trees from bootstrap samples and averages their outputs (Prasad et al., 2006). This approach reduces variance, improves generalization, and delivers stable, accurate predictions across diverse regression tasks (Brieuc et al., 2018). ERT is an ensemble method like RF but adds randomness by selecting both random features and random split points (Geurts et al., 2006). This produces shallower, more diverse trees, increasing bias but reducing variance, which improves stability and generalization (Zhou et al., 2025). XGBoost is an advanced gradient boosting method that builds trees sequentially and incorporates regularization to control complexity and reduce overfitting (Chen and Guestrin, 2016). It uses a second-order Taylor expansion for efficient and accurate loss optimization. LightGBM is a GBDT-based algorithm optimized for speed and scalability (Ke et al., 2017). It uses Gradient-based One-Sided Sampling and Exclusive Feature Bundling to accelerate training, and a leaf-wise growth strategy for higher accuracy with fewer iterations. Overfitting is controlled through constraints like max depth and minimum samples per leaf, enabling efficient, large-scale

Table 2
Summary of machine learning models.

No.	Model	Category
1	ANN	Classical
2	SVM	Classical
3	RF	Ensemble – Bagging
4	ERT	Ensemble – Bagging
5	XGBoost	Ensemble – Boosting
6	LightGBM	Ensemble – Boosting

predictive modeling. Both XGBoost and LightGBM are high-performance gradient boosting algorithms known for their accuracy and efficiency on structured data.

2.3. Evaluation metrics

Model performance was evaluated using four metrics: MAE, RMSE, MAPE, and R^2, as shown in Eq. (2) to Eq. (5). MAE measures the average magnitude of prediction errors without considering direction and directly reflects the typical deviation between predicted (y_{pre}) and actual values (y_{test}), providing an intuitive sense of accuracy in the same unit as the target variable. RMSE calculates the square root of the average squared differences between predictions and actual values, penalizing larger errors more heavily and making it particularly sensitive to outliers while identifying models that minimize large deviations. MAPE expresses prediction error as a percentage of actual values, allowing scale-independent comparison and facilitating interpretation of accuracy in relative terms. R^2 indicates the proportion of variance in the target variable explained by the model, with higher values suggesting the model captures patterns and trends. Lower MAE, RMSE, and MAPE indicate higher accuracy, while an R^2 near one signifies a better fit.

$$RMSE = \sqrt{\frac{1}{n}\sum_{i=1}^{n}\left(y_{i,pre} - y_{i,test}\right)^2} \tag{2}$$

$$MAPE = \frac{1}{n}\sum_{i=1}^{n}\left|\frac{y_{i,pre} - y_{i,test}}{y_{i,test}}\right| \times 100\% \tag{3}$$

$$MAE = \frac{1}{n}\sum_{i=1}^{n}\left|y_{i,pre} - y_{i,test}\right| \tag{4}$$

$$R^2 = 1 - \frac{\sum_{i=1}^{n}\left(y_{i,test} - y_{i,pre}\right)^2}{\sum_{i=1}^{n}\left(y_{i,test} - \bar{y}\right)^2} \tag{5}$$

where $\bar{y}$ represents the mean compressive strength; n indicates the total number of observations.

2.4. Hyperparameter tuning

Hyperparameters are configuration settings that influence the performance of machine learning models and must be specified prior to training. Common tuning methods include Grid Search (Sun et al., 2021a), Random Search (Bergstra and Bengio, 2012), and Bayesian Optimization (Wu et al., 2019). Given the dataset size (1209 samples), Grid Search and Random Search are computationally inefficient, so this study employs Bayesian Optimization for its ability to explore complex search spaces with fewer evaluations (Wu et al., 2019). It iteratively evaluates hyperparameter combinations, each informed by prior results, enabling faster convergence toward optimal parameters. By building a surrogate model of the target function, Bayesian Optimization directs the search to promising regions, balancing exploration and exploitation. Here, it is combined with 10-fold cross-validation with stratification to identify the optimal hyperparameters. The pre-defined search space for ANN, SVM, RF, ERT, XGBoost, and LightGBM is listed in Table A1 (see Appendix). In 10-fold cross-validation, the training data is split into ten subsets; each subset serves once for validation while the remaining nine are used for training (Guo et al., 2024).

2.5. SHAP-based model explanation

Machine learning algorithms often lack interpretability, limiting transparency in decision-making. To address this, SHAP, rooted in cooperative game theory, is used to provide global and local interpretability by quantifying each input variable's contribution to the output (Che et al., 2017). In this study, SHAP analyzes feature importance to enhance model reliability. SHAP analysis is employed with three primary objectives: (1) Quantifying the influence of individual features across the entire dataset, thereby identifying which input variables have the greatest impact on model predictions; (2) Exploring correlations between parameter values through SHAP dependence plots, which reveal how changes in one feature's value influence the predicted outcome in conjunction with other features. (3) Offering insights into complex relationships that are not evident when considering features in isolation. The results are shown in Section 3.4.

2.6. Economy and environmental impacts

LCA plays a key role in evaluating the true sustainability of rubberized concrete by accounting for economy (cost analysis) and environmental impacts (carbon emission and energy efficiency). In this research, a cradle-to-gate boundary is applied to assess the environmental impacts of rubberized concrete. The inventory data utilized for the LCA can be found in Table 3. It outlines the cost, carbon emission, and embodied energy associated with each raw material employed in the production of rubberized concrete. The strength-normalized cost, carbon footprint, and energy consumption were also computed, aimed at evaluating the cost-effectiveness, carbon emissions, and energy efficiency of rubberized concrete production. These evaluations were accomplished through combining the compressive strength measured at 28 days with the corresponding unit costs, emission levels, and energy requirements.

By utilizing the inventory information provided in Table 3, the required production cost, carbon emissions, energy usage during the production of per cubic meter of rubberized concrete were evaluated using Eq. (6) to Eq. (8) (Guo et al., 2023b):

$$M = \sum_{i=1}^{n} m_i r_i \tag{6}$$

$$C = \sum_{i=1}^{n} c_i r_i \tag{7}$$

$$E = \sum_{i=1}^{n} e_i r_i \tag{8}$$

where M, C, and E represent the unit manufacturing cost, the generated CO_2 emissions, and the total energy required during the production of 1 cubic meter of rubberized concrete, respectively; m_i, c_i, and, e_i symbolize

Table 3
Inventory data for each raw ingredient used in LCA.

No.	Materials	Cost ($/kg)	Carbon footprint (kg/kg)	Energy consumption (MJ/kg)
1	Cement	0.084 (Alsalman et al., 2020)	0.820 (Sun et al., 2021b)	4.73 (Chiaia et al., 2014)
2	Silica fume	0.800 (Guo et al., 2023a)	0.014 (Guo et al., 2023a)	0.018 (Mahjoubi et al., 2025)
3	Fine aggregate	0.010 (Guo et al., 2023a)	0.002 (Guo et al., 2023a)	0.022 (Mahjoubi et al., 2025)
4	Coarse aggregate	0.014 (Guo et al., 2023a)	0.004 (Guo et al., 2023a)	0.022 (Mahjoubi et al., 2025)
5	Waste rubber	0.0035 (Mahjoubi et al., 2025)	0.0042 (Chen et al., 2023)	0.014 (Sinkhonde, 2023)
6	Superplasticizer	3.0 (Mahjoubi et al., 2021)	0.72 (Mahjoubi et al., 2021)	9.0 (Mahjoubi et al., 2021)
7	Water	0.001 (Guo et al., 2023a)	0.0003 (Guo et al., 2023a)	0.00574 (Chiaia et al., 2014)

the unit cost, the CO_2 emissions, and the energy consumption used to produce the *i*th component *(i = 1, 2, 3, …, n)*, respectively; and r_i indicates the mass of the *i*th ingredient.

3. Results and discussion

3.1. Hyperparameter tuning results

After training and evaluating each model, the variation of the test set R^2 scores during the Bayesian optimization process was recorded with respect to the number of iterations, as illustrated in Fig. 3. It is evident that, apart from the ANN model, the R^2 values of the other 5 models reached stability after 200 iterations, all surpassing 0.9. Finally, the optimal hyperparameter values are selected based on the highest average predictive accuracy. These values are presented in Table A2 (see Appendix). Since LightGBM achieved the highest predictive accuracy among all tested models, Fig. A2 (see Appendix) presents its score plot, with the shaded region indicating the minimum–maximum range of R^2 values obtained across the 10 folds at each optimization iteration. This visualization not only highlights the model's overall performance but also reveals the variability in accuracy across folds, offering insights into its stability and robustness during hyperparameter tuning.

3.2. Prediction process

The first sample from the dataset has been randomly selected to illustrate the forecasting procedures of ANN, SVM, RF, ERT, XGBoost, and LightGBM, as shown in Fig. 4. The first sample is $w/c = 0.35$, $C_R = 0$ kg/m^3, $S_R = 0$ mm, $C_C = 400$ kg/m3, $C_{FA} = 769$ kg/m3, $C_{CA} = 1149$ kg/m3, $sf/c = 0$ %, $C_S = 5.9$ kg/m3, $T_C = 28$ days, and $f_C = 64.17$ MPa. In the figure, red and blue bars indicate the beneficial and adverse effects of individual features on the forecasted compressive strength, with their lengths indicating the absolute Shapley values for each feature. It is evident that all the models consistently identify C_R, w/c, C_{FA} as the top three factors influencing compressive strength. This is evidenced by the longer bars for these parameters compared to other features. Since adding rubber decreases compressive strength, its absence has a positive effect. The models also agree that a lower w/c (0.35) and a higher C_{CA} (1149.0 kg/m^3) positively contribute to compressive strength. In contrast, the effects of S_R, sf/c, C_S and C_C are less important. Through the incorporation of base values, positive impacts, and negative impacts, these models collectively generate a conclusive forecast. It should be noted that there exist disparities in mixture ratios among samples. Some samples have content values below the mean SHAP, while others are higher.

According to Table 4, the anticipated compressive strengths from the ANN, SVM, RF, ERT, XGBoost, and LightGBM models are reported as 52.64 MPa, 63.17 MPa, 61.27 MPa, 62.32 MPa, 63.76 MPa, and 63.75 MPa, respectively. The discrepancies between the measured compressive strengths and the forecasts by these models are reported as −17.97 %, −1.56 %, −4.52 %, −2.88 %, −0.64 %, and −0.65 %, respectively. Apart from the ANN model, the absolute forecasting errors of the remaining five models fall below 5 %, reinforcing the efficacy and accuracy of machine learning techniques. By contrast, the effects of the maximum size of crumb rubber (S_R), ratio of silica fume to cement (sf/c), superplasticizer content (C_S) and content of cement (C_C) are less important. Through the incorporation of base values, positive impacts, and negative impacts, these models collectively generate a conclusive forecast.

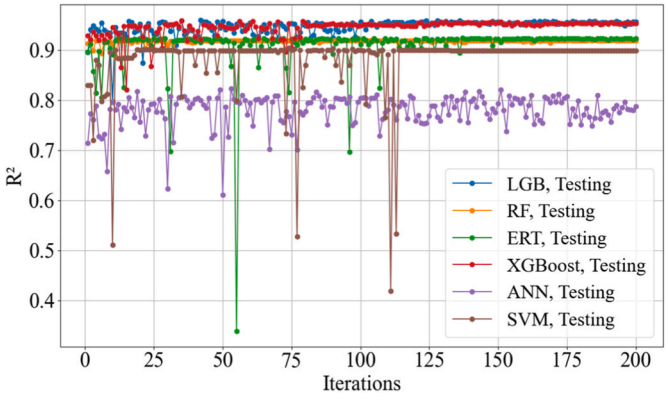

Fig. 3. R^2 scores of the six models changed with the number of iterations using the Bayesian optimization algorithm under 10-fold cross-validation.

3.3. Prediction performance

Fig. 5 illustrates the effectiveness of six machine learning algorithms. Except for the ANN model, all models achieved excellent predictive accuracy for rubberized concrete strength, achieving R^2 scores above 0.97. They also fulfill the ML standard of MAE being less than RMSE (Khan et al., 2022). Moreover, the five ML models exhibit robust training performance, with all RMSE values under 3. Notably, the ERT and LightGBM models demonstrate higher predictive accuracy on the training dataset, achieving the lowest RMSE and MAE values, with R^2 values both reaching 0.99. The RF and XGBoost models showed slightly lower performance, with higher error metrics and lower R^2 compared to ERT and LightGBM. In comparison, the accuracy of the SVM model is relatively low, but still acceptable given that its R^2 reached 0.97. Overall, the ANN model exhibited relatively lower efficiency compared to the other models, indicated by higher RMSE, MAPE, and MAE metrics, along with an R^2 of 0.87.

Fig. 6 shows the testing performance of six ML models. Except for ANN, all models achieved R^2 values above 0.91, indicating strong predictive accuracy. Given LightGBM's highest accuracy on the same dataset, the gap is more likely due to algorithmic differences rather than sample distribution limitations. Tree-based ensemble methods, particularly boosting algorithms such as LightGBM, capture complex nonlinear feature interactions, handle heterogeneous data, and mitigate overfitting through regularization. LightGBM outperformed other models mainly because its leaf-wise growth strategy with depth constraints captures complex feature interactions more effectively, while histogram-based binning reduces overfitting. SVM may struggle with high-dimensional regression unless its kernel is carefully tuned. Compared with bagging-based models (ERT/RF), it lowers bias by sequentially correcting errors, and compared with XGBoost, it can fit local patterns more precisely, making it better suited to the nonlinear relationships.

In this research, the risk of overfitting is considered low for two main reasons: (1) The model was trained on a large and diverse dataset that captures a wide range of mixture designs, and (2) the predictive performance remained consistently high across both the training and test sets.

Table 5 summarizes the model's prediction performance across three compressive strength intervals (0–30 MPa, 30–60 MPa, and 60–90 MPa), covering an overall strength range of 0–87 MPa. This breakdown facilitates the identification of potential overfitting or underfitting within specific intervals, which may result from data imbalance, as discussed in (Ali et al., 2023). Performance is classified as poor ($R^2 < 0.70$), medium ($0.70 \leq R^2 < 0.80$), and good ($R^2 \geq 0.80$).

Since the overall performance metrics exhibit the same trend, Table 4 reports only the R^2 and RMSE values. Across the three compressive strength ranges, model performance varied notably. LightGBM achieves consistently good results ($R^2 \geq 0.81$) and the highest accuracy in the high-strength range ($R^2 = 0.91$), followed by XGBoost, which performed strongly in the low and high ranges but was slightly weaker in the medium range. In contrast, ANN performed poorly in all ranges, particularly in the high-strength range, while SVR, RF, and ERT showed moderate to good results in the low and medium ranges but

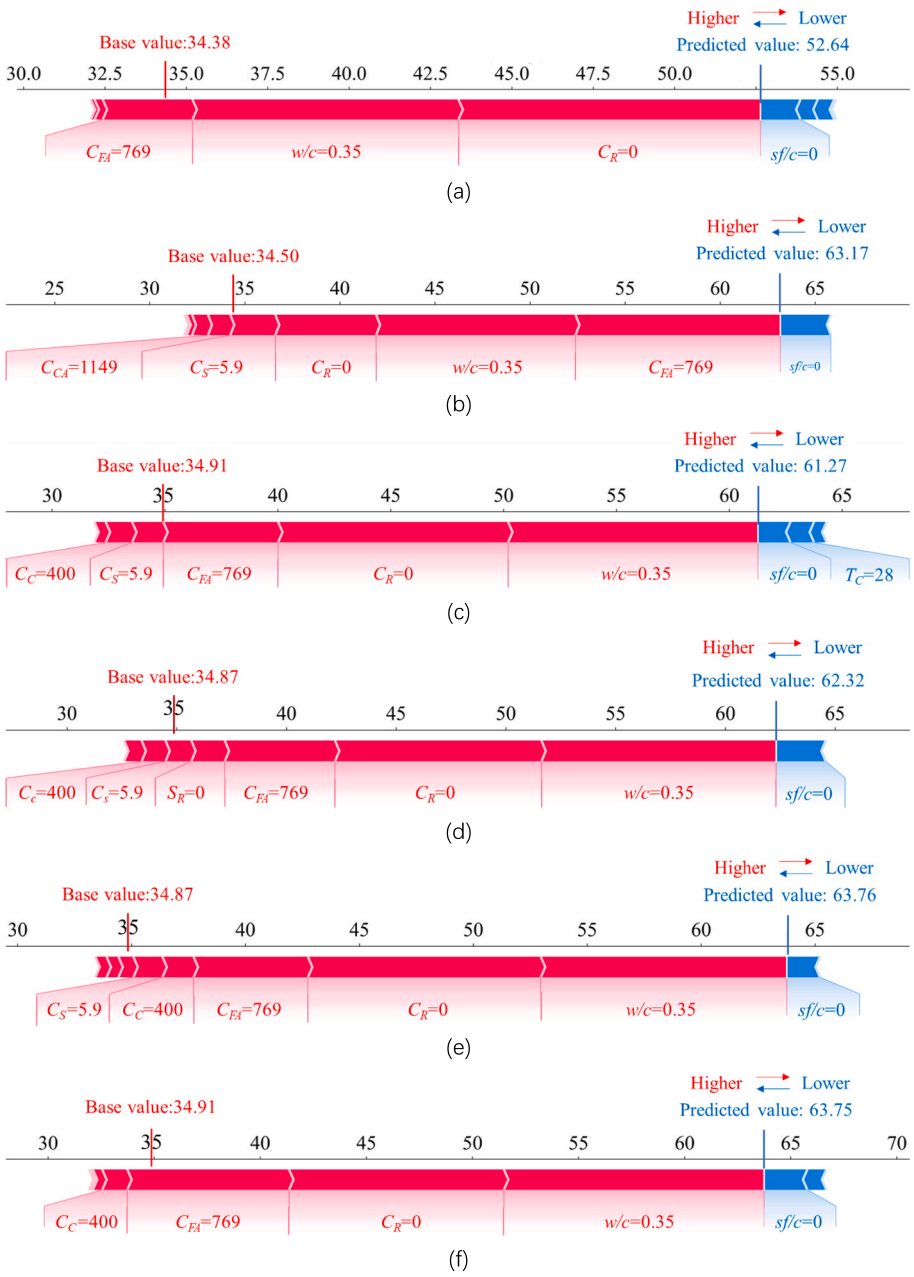

Fig. 4. Prediction process of different machine learning models: (a) ANN; (b) SVM; (c) RF; (d) ERT; (e) XGBoost; and (f) LightGBM.

Table 4
Actual and predicted compressive strength of the sample investigated.

Models	ANN	SVM	RF	ERT	XGBoost	LightGBM
Actual	64.17	64.17	64.17	64.17	64.17	64.17
Predicted	52.64	63.17	61.27	62.32	63.76	63.75
Error	−17.97 %	−1.56 %	−4.52 %	−2.88 %	−0.64 %	−0.65 %

suffered significant drops in the high range, likely due to data imbalance. Overall, LightGBM and XGBoost are not affected by the data imbalance problem.

3.4. Parametric analysis

3.4.1. Influence of individual features

SHAP analysis quantifies the contributions of each input variable to the predicted compressive strength of rubberized concrete for a specific instance (Kashem et al., 2024). Fig. 7 presents the SHAP values for each input variable across all samples, computed using the LightGBM model identified as optimal in Section 3.3. The figure includes pie charts of variable importance, bar chart presents the average SHAP values, and beeswarm plots showing feature impact distribution and magnitude. The model identifies the rubber content (C_R) as the most important factor, accounting for more than 30 % of the total impact. The combined impact of C_R and the w/c exceed 50 %. C_R reduces strength by replacing part of the aggregate, while w/c controls hydration and strength

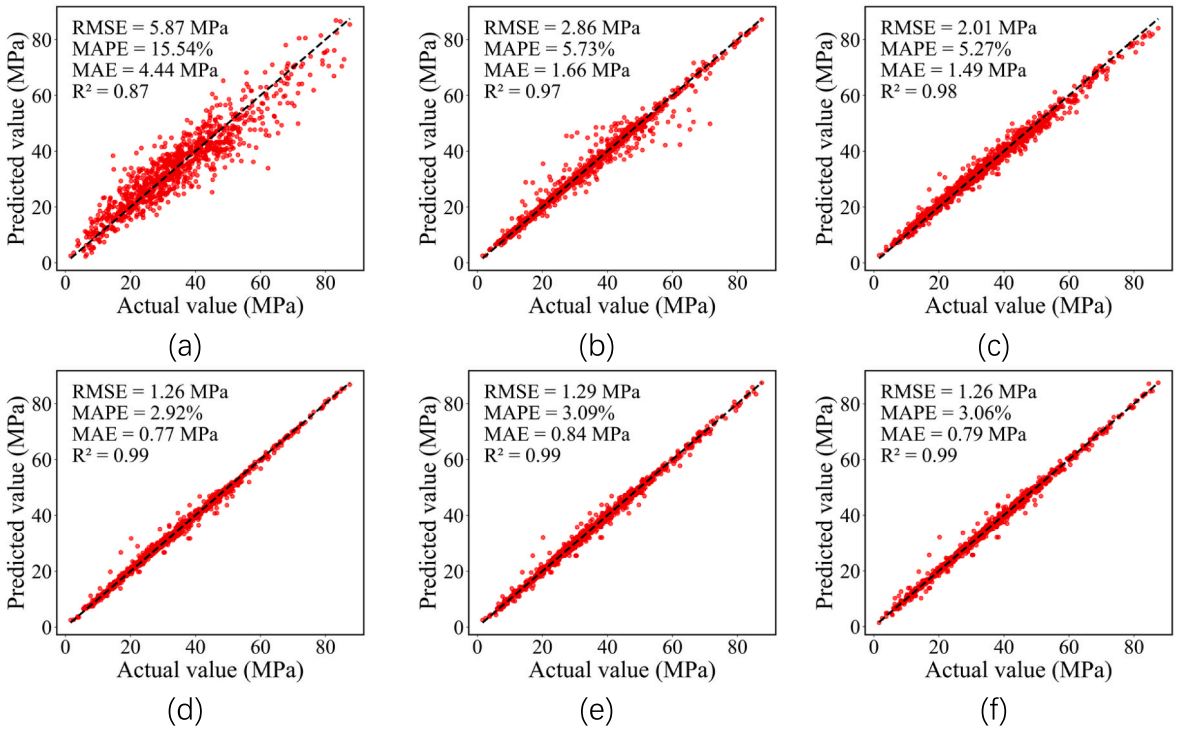

Fig. 5. Performance of ML models on training dataset: (a) ANN; (b) SVM; (c) RF; (d) ERT; (e) XGBoost; and (f) LightGBM.

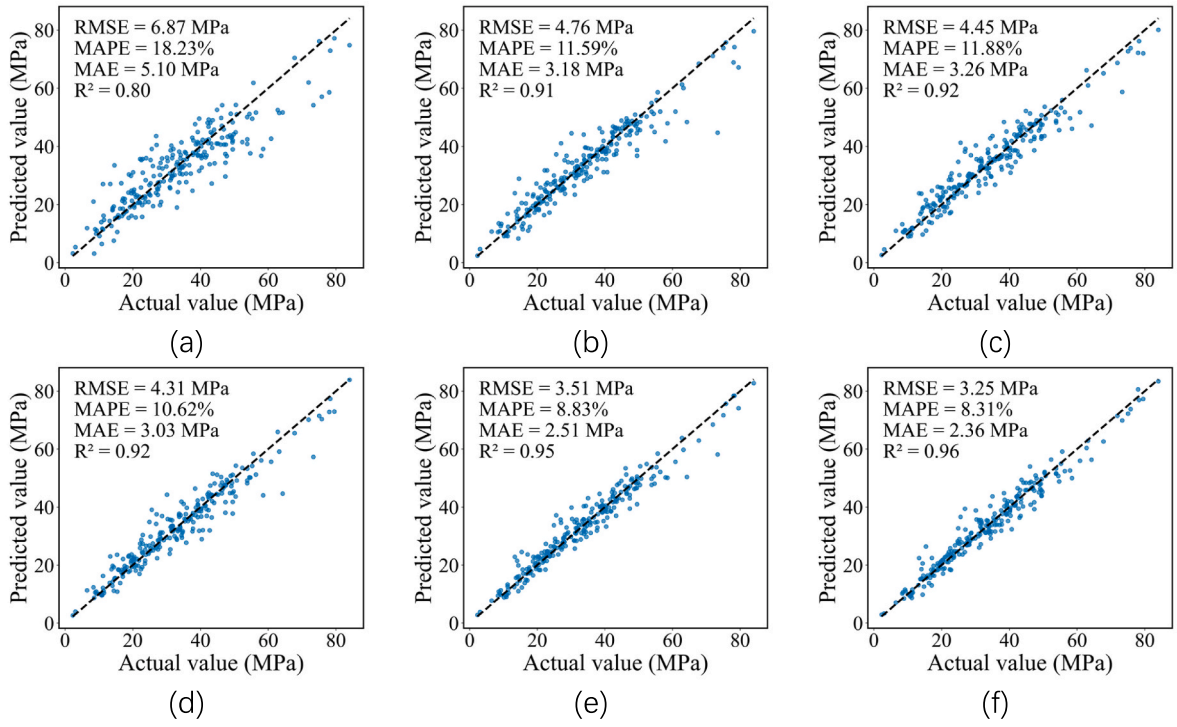

Fig. 6. Performance of ML models on testing dataset: (a) ANN; (b) SVM; (c) RF; (d) ERT; (e) XGBoost; and (f) LightGBM.

development, making both highly influential in the model (El-Gammal et al., 2010; Güneyisi et al., 2004). Fine aggregate content (C_{FA}), curing time (T_C), superplasticizer content (C_S), and the silica fume-to-cement ratio (sf/c) are categorized as medium-impact variables. Conversely, coarse aggregate content (C_{CA}), cement content (C_C), and the maximum size of crumb rubber (S_R) are consistently identified as the least impactful variables. The medium-impact features contribute 35.6 % to the model predictions, while the low-impact features contribute only 12.4 %.

The beeswarm plots show the distribution of SHAP values for each feature, with dots representing samples colored by feature value. Features are sorted by average SHAP impact. For the LightGBM model, rubber content (C_R) and water-to-cement ratio (w/c) are the most influential features. It also assigns high importance to the silica fume-to-

Table 5
Model performance in different compressive strength ranges.

Models	Ranges (MPa)	No. of data	R^2	RMSE (MPa)	Remark
ANN	0–30	102	0.29	6.09	Poor
	30–60	127	0.38	6.10	Poor
	60–90	13	−0.45	10.08	Poor
SVR	0–30	102	0.71	3.90	Medium
	30–60	127	0.69	4.31	Poor
	60–90	13	−0.07	8.66	Poor
RF	0–30	102	0.72	3.82	Medium
	30–60	127	0.74	3.99	Medium
	60–90	13	0.61	5.22	Poor
ERT	0–30	102	0.72	3.81	Medium
	30–60	127	0.70	4.24	Medium
	60–90	13	0.41	6.43	Poor
XGBoost	0–30	102	0.84	2.91	Good
	30–60	127	0.79	3.53	Medium
	60–90	13	0.89	2.80	Good
LightGBM	0–30	102	0.82	3.11	Good
	30–60	127	0.81	3.58	Good
	60–90	13	0.91	2.44	Good

cement ratio (sf/c), while curing time (T_C) shows a relatively strong impact. In contrast, cement content (C_C) and crumb rubber size (S_R) have minimal influence, possibly due to interactions with w/c and C_R, which reduce their SHAP contributions. This suggests that feature interactions play a critical role in determining variable importance within the model. It should be noted that disparities exist in mixture ratios across samples. For example, in some mixes the water-to-binder ratio or rubber content shows SHAP values lower than the mean SHAP, indicating that their contribution to strength prediction is less significant than the average level. Conversely, in other mixes these parameters exhibit SHAP values higher than the mean SHAP, suggesting that they play a more dominant role in influencing the prediction. This variability reflects the diversity of practical mixture designs and should be considered when interpreting the relative importance of features.

3.4.2. Correlation between the parameter values

SHAP values quantify the influence of each parameter on compressive strength from LightGBM model. As shown in Section 3.4.1, the top six features contribute about 90 % of the total impact on compressive strength. SHAP dependence plots for the six key features were fitted with LOWESS curves and ±0.5 standard deviation bands to show uncertainty. In contrast, fine aggregate (C_{FA}), rubber crumb size (S_R), and cement content (C_C) had minimal impact and showed no clear linear trends. These three variables were excluded due to their negligible impact, enabling parametric analysis of the relationship between feature values and their SHAP contributions. As depicted in Fig. 8(a) and (b), SHAP values for rubber content (C_R) and water-to-cement ratio (w/c) decrease with increasing feature values, indicating an inverse relationship with compressive strength. To minimize adverse effects, C_R should stay below 55.92 kg/m^3, and the w/c ratio under 0.4 to preserve the compressive strength. As depicted in Fig. 8(c)–8(f), curing time (T_C) silica fume-to-cement ratio (sf/c), fine aggregate content (C_{FA}) and superplasticizer content (C_S) exhibited positive correlations with compressive strength. Therefore, the following thresholds are recommended to enhance the compressive strength: $T_C > 26$ days, $sf/c > 2.5$ %, $C_{FA} > 642$ kg/m^3, and $C_S > 3.7$ kg/m^3, as these factors positively influence the compressive strength.

3.4.3. Pairwise SHAP interaction analysis

This section highlights SHAP's ability to capture the combined effects of feature interactions on model predictions. As shown in Fig. 9, pairwise interactions among nine input variables are visualized based on LightGBM outputs. Red dots indicate high values for both interacting features, while blue dots denote low values. The rubber content (C_R) and the water-to-cement ratio (w/c) show the strongest interaction effects, reflected by its broad SHAP value distribution and high variability. Individually, both high C_R and high w/c are known to detrimentally affect compressive strength (Topcu, 1995; Neville, 1995). However, for a given high w/c which already creates a more porous cement paste matrix, the addition of even a small amount of C_R leads to a disproportionately large drop in predicted strength. This is because the hydrophobic rubber particles further disrupt the hydration process and weaken the Interfacial Transition Zone within the already compromised matrix (Youssf et al., 2016; Thomas and Gupta, 2016b). At very low w/c ratios, the adverse effect of C_R is partially alleviated, suggesting a complex non-linear interdependence. Overall, the strong negative interaction between C_R and w/c is critical for practical applications: Utilizing rubber in concrete requires exceptionally tight control over w/c to avoid catastrophic losses in strength, which should be further underscored. In contrast, features like cement content (C_C) and crumb rubber size (S_R) exhibit low SHAP values with limited spread, indicating weak interaction influence. The minimal interaction for C_C suggests that increasing cement content generally improves strength predictably, regardless of the values of other features, as it is the primary binder. The weak influence of S_R is consistent with findings that the negative impact of rubber is more dominantly governed by its volume than its particle size (Guo et al., 2017). The interaction patterns are consistent with the trends observed in Fig. 8, in which the rubber content (C_R) and the water-to-cement ratio (w/c) have a substantial influence on compressive strength, whereas cement content (C_C) and crumb rubber size (S_R) contribute minimally.

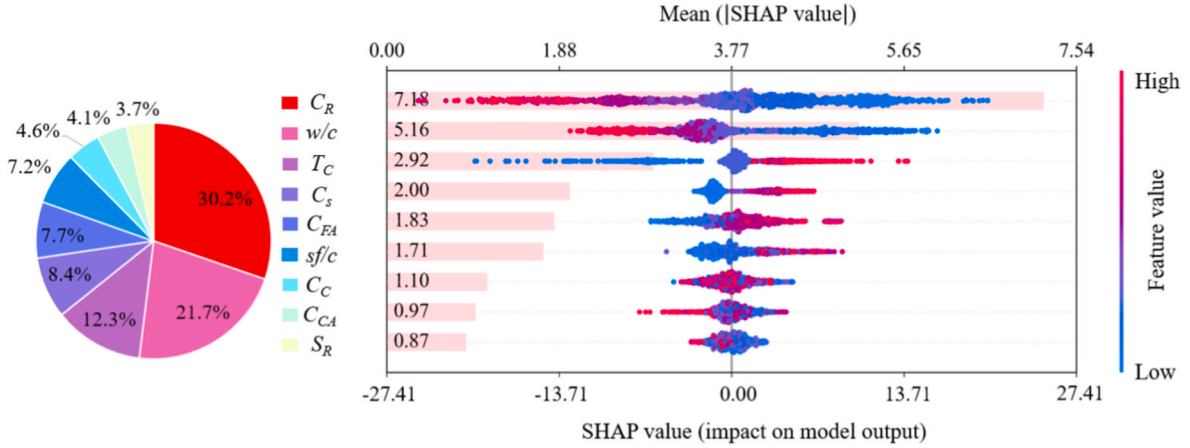

Fig. 7. SHAP-based interpretation of the outputs from LightGBM model.

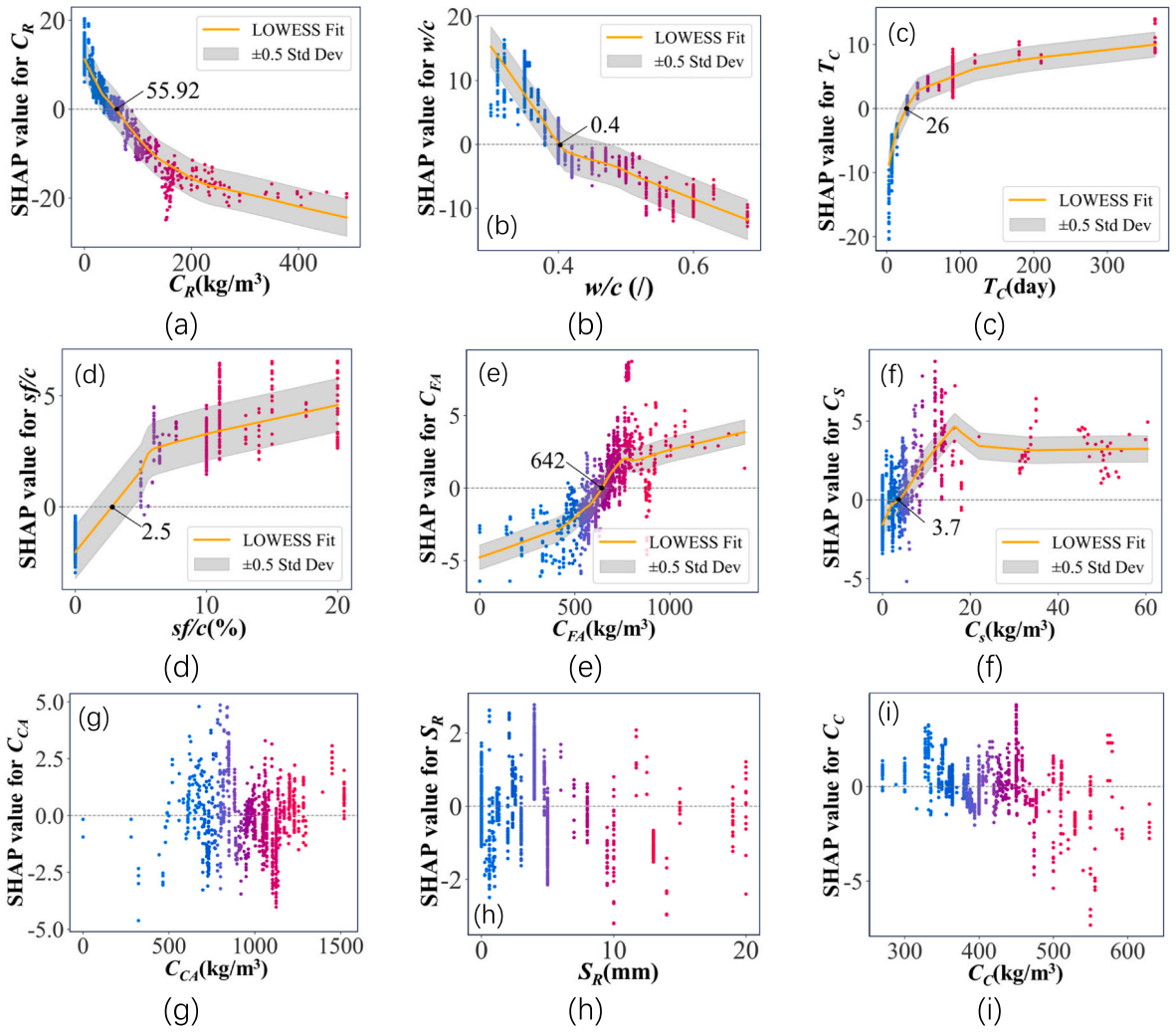

Fig. 8. SHAP value distribution of different input variables: (a) C_R; (b) w/c; (c) T_C; (d) sf/c; (e) C_{FA}; (f) C_S; (g) C_{CA}; (h) S_R; and (i) C_C.

3.5. Life cycle assessment and design recommendations

3.5.1. Cost analysis

The total cost analysis of 1209 rubberized concrete is shown in Fig. 10(a). Based on the LCA results, the cost of producing 1 m^3 of rubberized concrete ranges from $38.1 to $396.4, with an average of $79.7. The majority of rubberized concrete mixtures had a cost below $100 per cubic meter, indicating that rubberized concrete can be economically viable for large-scale construction applications when properly formulated. Fig. 10(b) presents the strength-normalized cost analysis of rubberized concrete cured for 28 days. The strength-normalized cost, representing the expense to achieve 1 MPa of compressive strength, varies between $1.02/MPa and $19.59/MPa, with average value of $2.81/MPa. Most rubberized concrete mixtures had a strength-normalized cost below $5/MPa.

3.5.2. Carbon emission

Fig. 11(a) shows the total carbon emission analysis for 1209 rubberized concrete mixtures. According to the LCA results, the carbon emission of producing 1 m^3 of rubberized concrete ranges from 237.2 kg to 552.6 kg, with an average of 365.8 kg. Most mixtures cost less than 400 kg per 1 m^3. Fig. 11(b) presents the strength-normalized carbon footprint for mixtures cured for 28 days, indicating the carbon emissions required to achieve 1 MPa of compressive strength. This value ranges from 4.1 kg/MPa to 132.0 kg/MPa, with an average of 14.0 kg/MPa. Very low compressive strengths, such as 3–5 MPa, lead to disproportionately high strength-normalized carbon footprints, often exceeding 130 kg/MPa. The majority of mixtures remained below 20 kg/MPa, with the lowest carbon footprint recorded at 4.1 kg/MPa.

3.5.3. Energy efficiency

Fig. 12(a) presents the total energy consumption analysis for 1209 rubberized concrete mixtures. Based on the LCA results, the energy required to produce 1 m^3 of rubberized concrete ranges from 1352.4 MJ to 3007.3 MJ, with an average of 2047.4 MJ. Most mixtures consume less than 400 kg of material per cubic meter. Fig. 12(b) shows the strength-normalized energy consumption for mixtures cured for 28 days, representing the energy needed to achieve 1 MPa of compressive strength. This metric ranges from 24.4 MJ/MPa to 760.0 MJ/MPa, with an average of 81.7 MJ/MPa. As with strength-normalized carbon emissions, very low compressive strengths (e.g., 3–5 MPa) result in disproportionately high energy consumption per unit strength, often exceeding 750 MJ/MPa. Most mixtures fall below 100 MJ/MPa, with the lowest recorded value at 24.4 MJ/MPa.

It should be pointed out that some mixes yield very high carbon footprint or energy consumption values when normalized by mechanical intensity, as shown in Figs. 11(b) and 12(b). These represent boundary conditions in the material design space. While such mixes may not be suitable for structural applications due to low strength, they remain relevant for non-structural uses, and as benchmarks for optimizing trade-offs between environmental impact and performance. These findings highlight the need to balance sustainability goals with

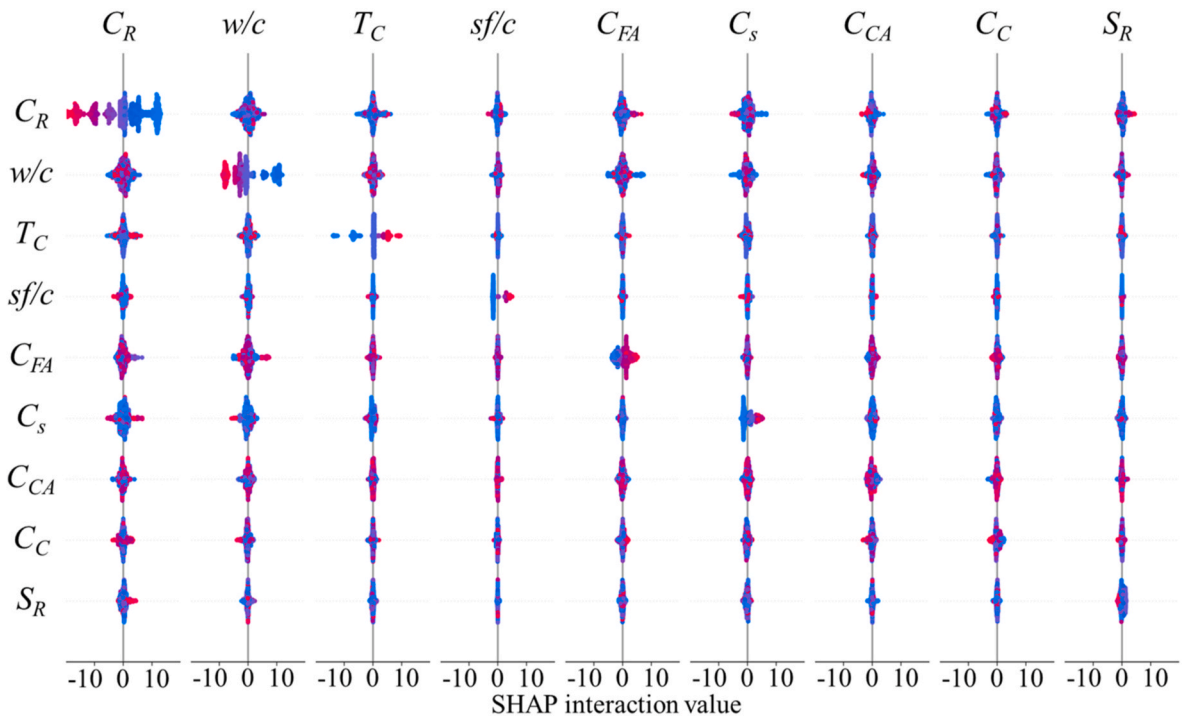

Fig. 9. SHAP interaction value plot for nine input features.

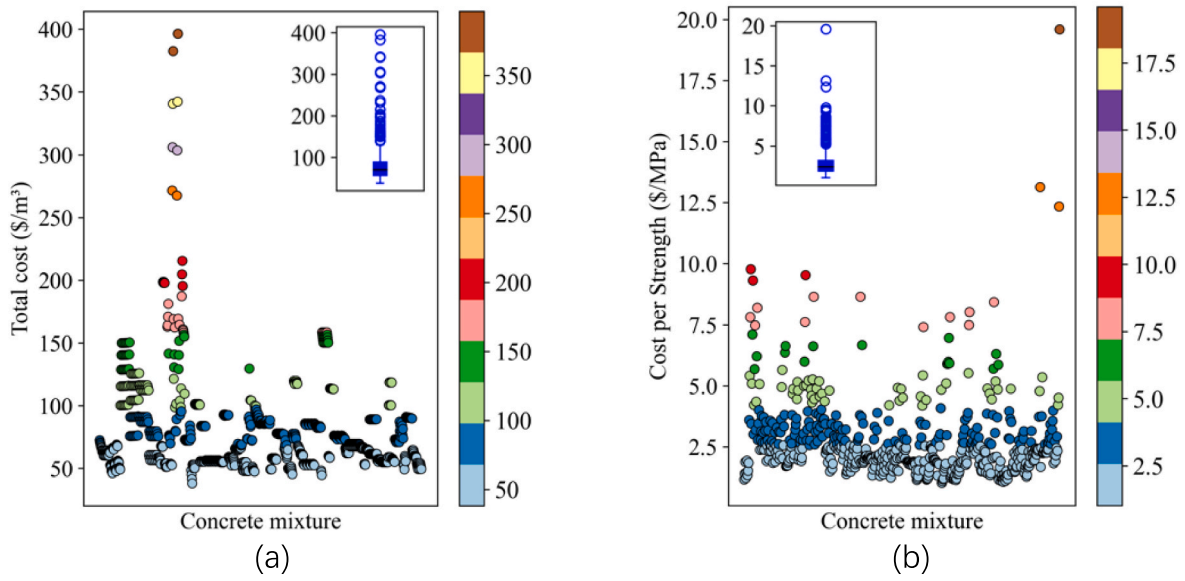

Fig. 10. Cost analysis of various rubberized concrete: (a) total cost; (b) strength-normalized cost.

functional requirements in concrete mix design.

3.5.4. Design recommendations

In rubberized concrete mixture design, a trade-off means balancing competing objectives, where improving one aspect often compromises another. For example, increasing rubber content improves cost efficiency and sustainability but decreases compressive strength, whereas increasing cement content enhances strength but raises both cost and emissions. It is challenging to identify an optimal solution that strikes a balance among all aspects. Fig. 13 illustrates the use of a 3D plot to identify the optimal rubberized concrete mixture. Each point in the plot represents a specific mix, allowing for a clear comparison across environmental and economic dimensions. When considering strength in the optimization, three indicators include cost, carbon emissions, and energy consumption are first normalized by compressive strength. Each of these three indicators was then normalized to a common scale of 0–1 using MinMaxScaler, which can eliminate the bias caused by differing magnitudes. The normalized values were then assigned equal weights of 0.33, reflecting balanced importance among economic and environmental objectives. After normalization and weight assignment, visualizing these three key performance indicators together enables the identification of trade-offs between cost-efficiency, sustainability, and strength. Mixtures with low values across all axes cluster near the origin, and the optimal design is highlighted as the point with the lowest combined impact.

Fig. 13(a) illustrates the use of a 3D plot to identify the optimal

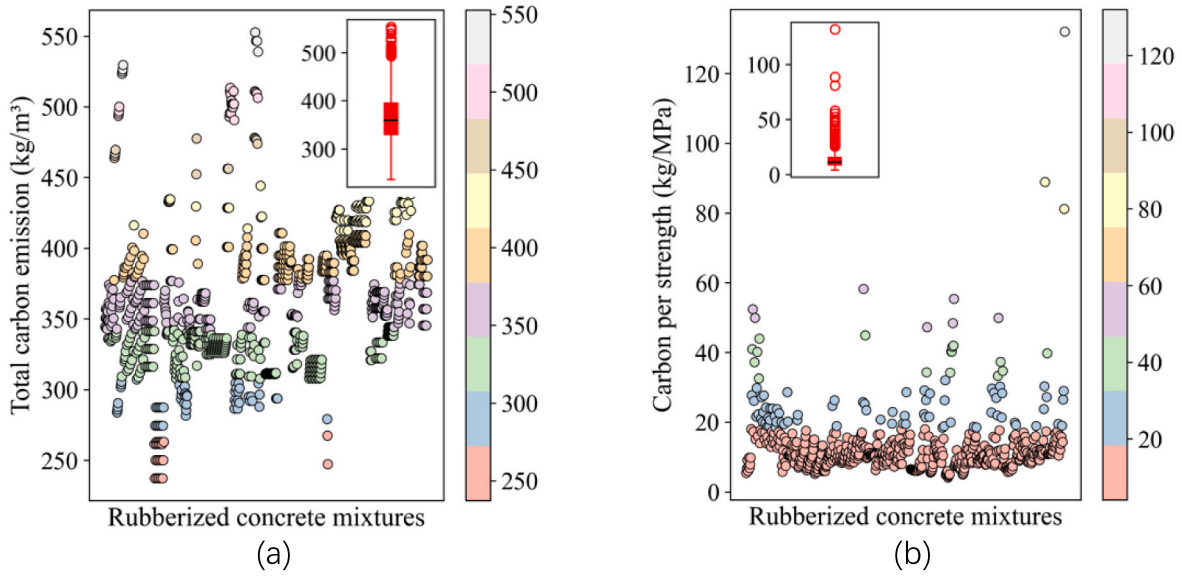

Fig. 11. Carbon analysis of various rubberized concrete: (a) total carbon emission; (b) strength-normalized carbon emission.

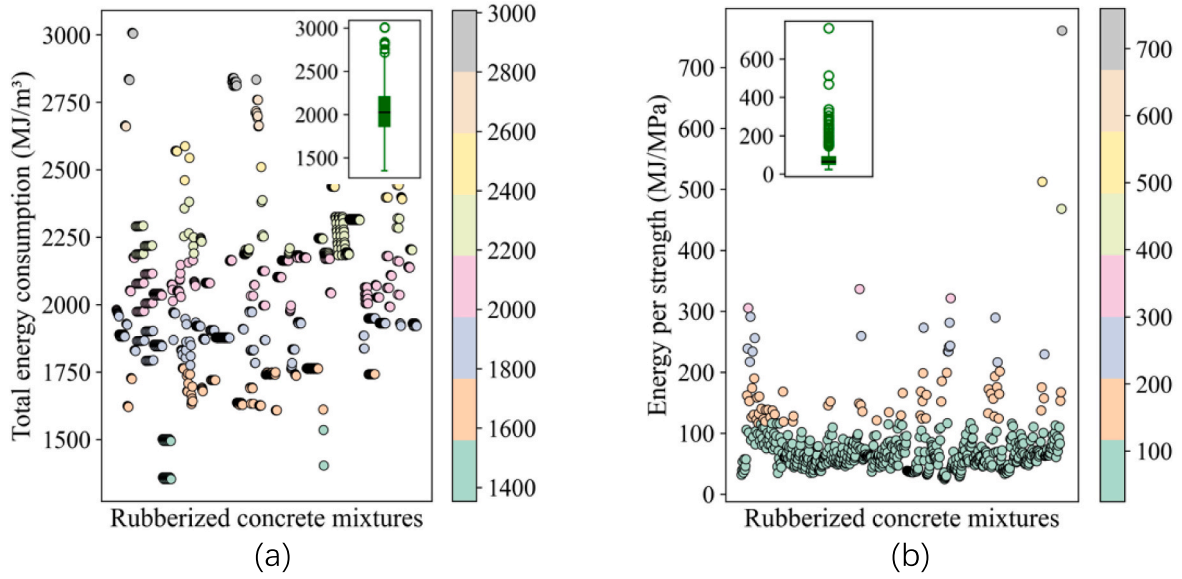

Fig. 12. Energy consumption analysis of various rubberized concrete: (a) total energy consumption; (b) strength-normalized energy consumption.

rubberized concrete mixture based on total cost, carbon emissions, and energy consumption. The optimal mixture, selected based on minimizing total cost, carbon emissions, and energy consumption, yields $44.64 in cost, 241.2 kg of CO_2 emissions, and 1402.6 MJ of energy use per cubic meter. This mixture consists of 288.20 kg of cement, 1005.00 kg of fine aggregate, 722.00 kg of coarse aggregate, 28.80 kg of rubber, and 172.92 kg of water, with no silica fume or superplasticizer included. The optimal mixture achieves a compressive strength of 24.5 MPa, sufficient to meet typical construction standards. Fig. 13(b) presents a 3D plot of the strength-normalized cost, carbon emission, and energy consumption for each concrete mixture. When considering the 28-day compressive strength, the optimal rubberized concrete mixture achieves a cost of $0.76 per MPa, a carbon emission of 4.35 kg per MPa, and an energy consumption of 24.95 MJ per MPa. This mixture consists of 288.2 kg of cement, 1005.0 kg of fine aggregate, 722.0 kg of coarse aggregate, 28.8 kg rubber, and 172.9 kg of water, with no inclusion of silica fume and superplasticizer. It delivers a 70.6 MPa strength, demonstrating strong mechanical strength with minimized environmental and economic impact.

3.5.5. *Comparison between rubberized and conventional concrete*

Fig. 14 provides a comparison between rubberized concrete and conventional concrete based on total cost, carbon emission, and energy consumption, including their strength-normalized equivalents, with data from the whole dataset. In the dataset of 1209 samples, those containing 0 % rubber content were selected as conventional concrete (control samples), while samples in which fine aggregate was replaced with waste rubber were classified as rubberized concrete. Although rubberized concrete is often promoted for its potential environmental and economic benefits, the results from all six comparative plots, covering total cost, carbon emission, energy consumption, and their strength-normalized forms do not support this assumption. Rubberized concrete mixtures exhibit comparable cost, carbon emissions, and energy consumption levels to conventional concrete across all evaluated metrics, as shown in Fig. 14(a)–14(c). Fig. 14(d)–14(f) compare the strength-normalized cost, carbon emissions, and energy consumption of

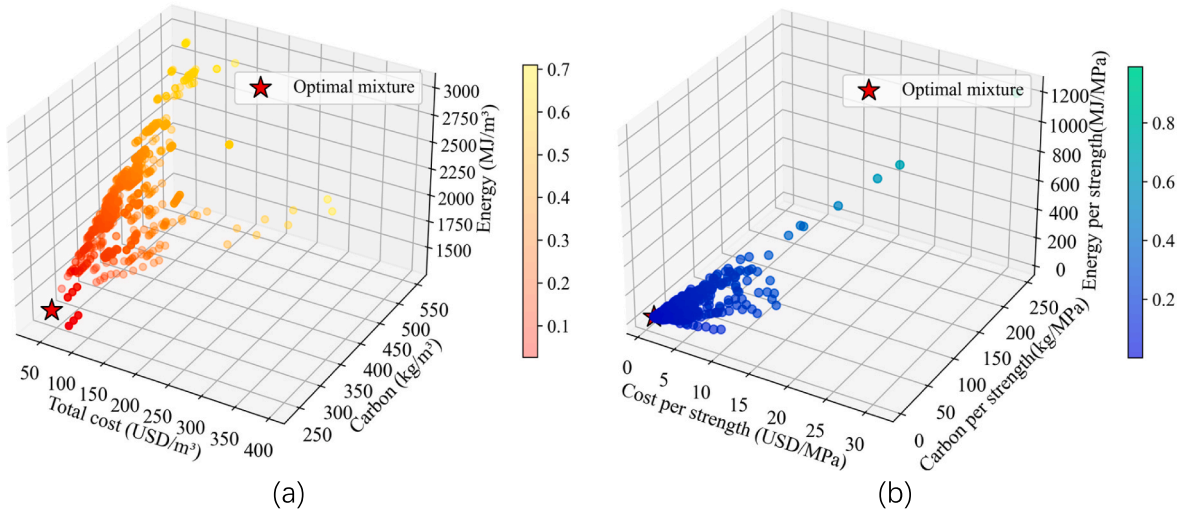

Fig. 13. Evaluation of optimal design based on: (a) total cost, carbon emission, and energy consumption for each mixture; (b) strength-normalized cost, carbon emission, and energy consumption for each mixture.

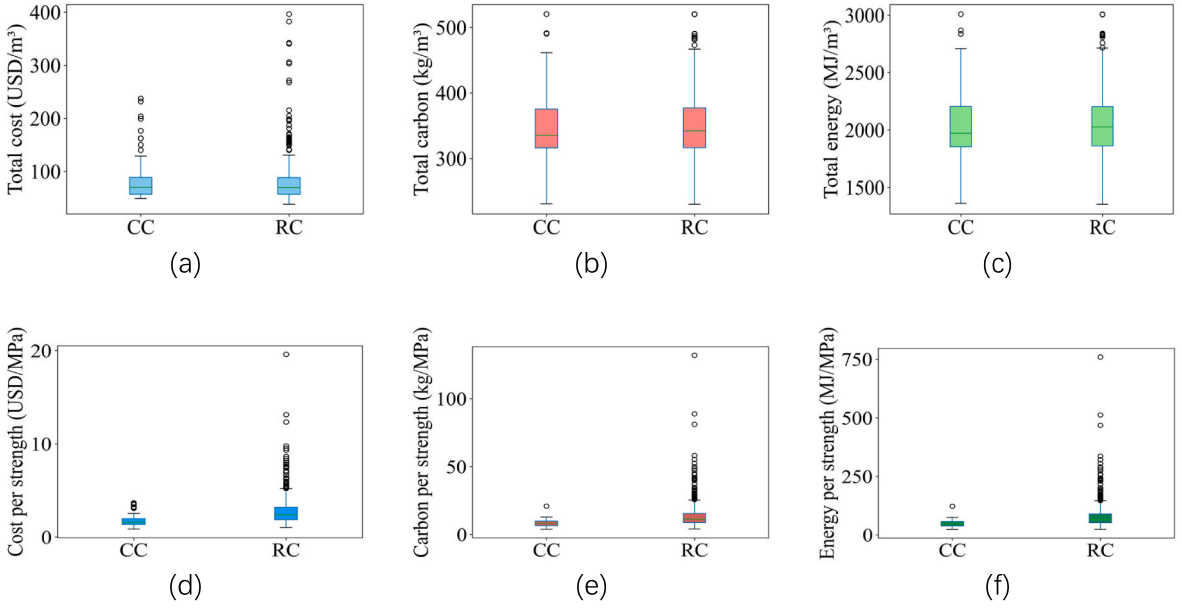

Fig. 14. Comparison of rubberized and conventional concrete in terms of: (a) cost; (b) carbon emission; (c) energy consumption; (d) strength-normalized cost; (e) strength-normalized carbon emission; (f) strength-normalized energy consumption.

rubberized concrete with those of conventional concrete. In many cases, they showed greater variability and higher values, especially in strength-normalized indicators. The higher energy and carbon emissions per MPa observed in rubberized mixtures are likely due to their lower compressive strength, which inflates normalized values. Additionally, rubber can disrupt particle packing and increase the superplasticizer demand, as superplasticizer contributes more to the economic and environmental impacts. This is consistent when incorporating other SCMs into normal concrete, such as fly ash, slag, and rice husk (Sathiparan and Subramaniam, 2025; Chowdhurya et al., 2025; Adegbemileke et al., 2024). When strength is a key design criterion, rubberized concrete may not offer a clear sustainability advantage.

3.5.6. *Effect of high-impact factors*

As illustrated in Fig. 7, rubber content (C_R) and water-to-cement ratio (w/c) are the two high-impact factors on compressive strength, accumulatively accounting for over 50 % of the total contribution. Therefore, this section is exclusively focused on these two high-impact factors.

Comparable findings are observed when examining data from a specific study (Xue et al., 2022). Fig. 15 presents the total cost, total carbon emissions, and total energy consumption, along with their strength-normalized counterparts, for mixtures incorporating up to 30 % rubber content (C_R) as a replacement for fine aggregate. The results indicate that while the total cost, carbon emissions, and energy consumption show only minor reductions with increasing crumb rubber replacement levels, the strength-normalized indicators exhibit a different trend. The total cost decreases slightly from 70.97 $ to 66.49 $, but the cost per unit compressive strength increases from 1.18 $/MPa to 1.93 $/MPa. This suggests that although the material cost is marginally reduced, the strength loss outweighs the savings, leading to higher cost efficiency penalties. Total carbon emissions remain nearly constant, indicating that rubber addition does not significantly reduce embodied carbon on a mass basis. The strength-normalized carbon footprint rises

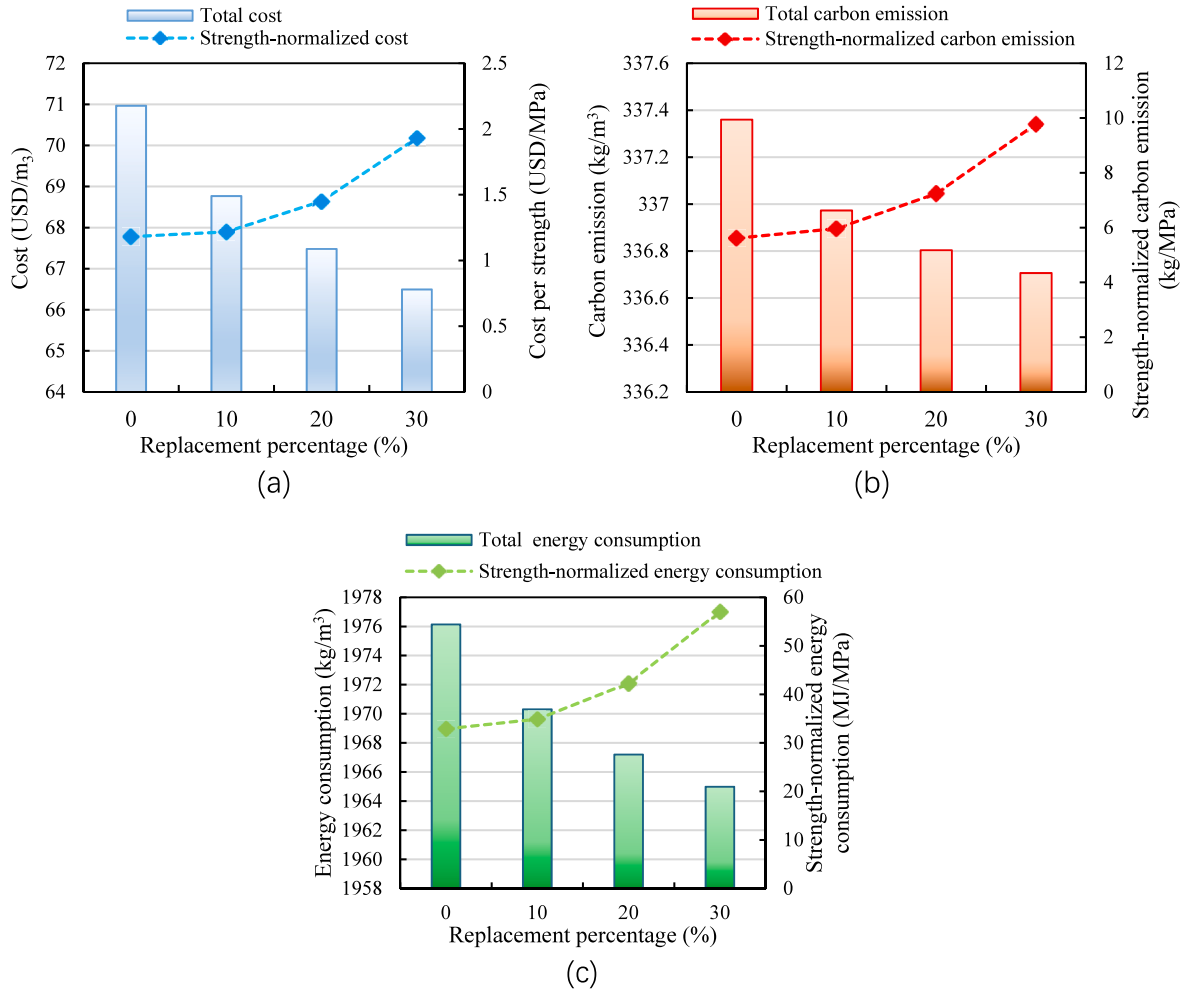

Fig. 15. Sustainability analysis of 0–30 % rubber content (C_R) in concrete: (a) cost; (b) carbon emission; and (c) energy consumption.

from 5.62 kg CO_2/MPa to 9.78 kg CO_2/MPa, reflecting the reduced mechanical performance. The total energy demand drops from 1976 MJ to 1965 MJ, but the energy consumption per MPa increases from 32.89 MJ/MPa to 57.07 MJ/MPa, again highlighting the detrimental effect of strength reduction on efficiency metrics.

Similarly, for the water-to-cement ratio (*w/c*), as indicated in Table 3, the cost, carbon footprint, and energy consumption of water are substantially lower than those of cement. Therefore, an increase in *w/c* reduces total cost, carbon emission, and energy consumption of the rubberized concrete mixture. In addition, Fig. 8(b) shows an obvious negative correlation between the water-cement ratio (*w/c*) and compressive strength. Consequently, an increase in *w/c* leads to higher strength-normalized values (cost/MPa, CO_2/MPa, and MJ/MPa) due to the corresponding decrease in strength. This finding further enhances the interaction revealed by SHAP analysis, linking mix design parameters directly to sustainability indicators.

3.6. Discussions

3.6.1. Repeatability and reproducibility

The repeatability and reproducibility of the presented analyses are primarily supported by three factors: (1) Dataset transparency and accessibility: The complete dataset of 1209 rubberized concrete samples, including input variables, standardized compressive strengths, and calculation procedures, has been made openly available via Mendeley Data, enabling independent researchers to directly re-run the analyses. (2) Standardized preprocessing and model training procedures, where all preprocessing steps such as Maximum-Absolute normalization (Section 2.1.1), 80/20 train–test split with a fixed random seed (Section 2.1.1), and 10-fold cross-validation are applied (Section 2.4), and model hyperparameter ranges are explicitly documented (Table A1), ensuring that the same dataset and settings will yield identical results if re-executed. (3) Model interpretability and parameter reporting: full disclosure of optimal hyperparameters for each machine learning model, together with the SHAP-based interpretation workflow, allows precise replication of the training process and interpretation outputs.

3.6.2. Limitations and future research

The data used in this study were sourced from existing literature, which introduced several inconsistencies across key dimensions, including material types, particle size distributions, detailed chemical compositions, geographic origins, and reporting formats. These inconsistencies reduce the reliability and comparability of performance assessments, potentially limiting the generalizability of the findings. Additionally, while this study focused on predicting the compressive strength of rubberized concrete, this property alone does not fully reflect the material's performance potential. Rubberized concrete is often valued not only for its load-bearing capacity but also for its enhanced impact resistance, durability, energy absorption, and long-term deformation characteristics, especially in applications such as pavements, seismic zones, and protective structures.

To address these limitations, there is an urgent need for targeted research aimed at developing a standardized, region-specific database tailored to rubberized concrete. Such a resource would enhance the

consistency and accuracy of performance evaluations, support regional optimization of mix designs, and enable more data-driven decisions in both material selection and engineering applications. Furthermore, future data collection efforts should expand beyond compressive strength to include a broader range of mechanical and durability-related properties, such as impact resistance, energy absorption, and long-term performance indicators, to better capture the full behavior and application potential of rubberized concrete.

To enhance the practical applicability of AI models in rubberized concrete research, future studies should focus on integrating high-dimensional, multi-source datasets. This includes not only traditional mix design variables but also a broader range of supplementary cementitious materials such as fly ash, slag, and rice husk ash, along with detailed physical and chemical properties of raw ingredients, including particle size distribution, surface area, and oxide composition. Such comprehensive data is essential for capturing complex nonlinear interactions resulting from the combined use of rubber aggregates and SCMs. Employing customized or hybrid machine learning algorithms that can effectively process these multidimensional inputs will improve model robustness, generalizability, and interpretability, ultimately supporting more reliable and sustainable concrete design.

Furthermore, the predictive model and the mechanisms it reveals are derived from historical experimental data. Although the high accuracy ($R^2 > 0.96$ on the test set) prediction result confirms a strong alignment with the compiled experimental results, future work will include targeted experimental programs to validate model predictions at critical boundary conditions and to physically verify the interaction mechanisms identified by SHAP analysis. This step is essential to bridge data-driven insights with direct experimental confirmation, thereby enhancing the model's reliability for practical applications.

Additionally, the input features considered in this study were confined to the conventional mixture proportions of rubberized concrete. While methods such as NaOH solution modification and silane coupling agent treatment are recognized for enhancing the rubber-cement matrix interface (Chen et al., 2019; Li et al., 2016b) and can indirectly influence compressive strength, these parameters fall beyond the present scope. Future research will explicitly incorporate these pretreatment techniques to expand the model's capability and provide more comprehensive guidance for performance-oriented mix design.

4. Conclusion

This research innovatively integrates LCA into the ML workflow to establish a ML-LCA integration framework that effectively links mechanical performance prediction with sustainability evaluation. By constructing the largest known dataset of 1209 samples, incorporating SHAP-based interpretation, and employing strength-normalized LCA, the study offers not only a robust tool for optimizing mix designs but also a new decision-support approach for designing eco-efficient rubberized concrete mixtures. The findings demonstrate the high predictive accuracy of ensemble learning models and provide critical insights into the environmental and economic implications of rubber inclusion in concrete. However, while rubberized concrete offers benefits in terms of waste recycling and mechanical toughness, it does not inherently enhance sustainability when strength is considered as a normalizing criterion. Based on the above discussions, the following sections present the key findings, research limitations, and future research directions.

- LightGBM has the best performance, with an R^2 value exceeding 0.96 on testing dataset, a MAPE of 8.31 %, a MAE of 2.36 MPa, and a RMSE of 3.25 MPa. SHAP analysis indicated that the rubber content (C_R) and water-to-cement ratio (w/c) were the two most influential features on compressive strength, with their combined contribution exceeding 50 %. To enhance compressive strength, it is recommended that the C_R content should be maintained below 55.92 kg/m^3, the w/c ratio should not exceed 0.4.
- Cost, carbon, and energy consumption for rubberized concrete were comparable to conventional concrete. When normalized by strength, rubberized mixtures often performed worse due to lower compressive strength. The optimal mix design identified in this study achieves a high compressive strength of 70.6 MPa with superior sustainability metrics, including a low cost of $0.76/MPa, carbon emissions of 4.35 kg/MPa, and energy consumption of 24.95 MJ/MPa. These capabilities make the framework applicable in real-world scenarios, such as optimizing pavement materials, precast elements, or environmentally friendly concrete products, especially when tailored to performance-based or green construction standards.
- The data used in this study were obtained from existing literature, which exhibited inconsistencies in material types, particle size distribution, detailed chemical compositions, geographic origins, and reporting standards. These variations compromise the reliability of performance assessments. Also, this study focused on compressive strength, but for rubberized concrete, key properties like impact resistance, durability, energy absorption, and long-term deformation are equally important.
- Therefore, there is an urgent need for targeted research to establish a standardized, region-specific database for rubberized concrete. Such a database would improve the consistency and accuracy of evaluations, thereby enabling more informed decisions in material selection and mix design. Moreover, future datasets should include additional target properties such as impact resistance, durability, and energy absorption. The design system also needs to be verified in the real-world applications or construction project or actual construction projects to ensure its practicality, robustness, and ability to meet performance requirements under realistic operating conditions.

CRediT authorship contribution statement

Xiao Tan: Writing – review & editing, Writing – original draft, Project administration, Methodology, Funding acquisition, Conceptualization. **Jianglei Xing:** Visualization, Investigation, Formal analysis, Data curation. **Yuan Wang:** Writing – review & editing, Project administration, Funding acquisition. **Haotian Qiu:** Validation, Data curation. **Soroush Mahjoubi:** Writing – review & editing, Validation. **Pengwei Guo:** Writing – review & editing, Methodology, Investigation, Data curation.

Declaration of Competing Interest

The authors declare the following financial interests/personal relationships which may be considered as potential competing interests: Xiao Tan reports financial support was provided by National Natural Science Foundation of China (Grant No: 52508343), Basic Research Program of Jiangsu (Grant No: BK20251486), and Fundamental Research Funds for the Central Universities (Grant No: B250201004).

Yuan Wang reports financial support was provided by National Natural Science Foundation of China (Grant No: U23B20144, 52209129).

Acknowledgement

The authors are grateful for the financial support provided by the Fundamental Research Funds for the Central Universities (Grant No: B250201004), the National Natural Science Foundation of China (Grant No: 52508343, U23B20144, 52209129), and the Basic Research Program of Jiangsu (Grant No: BK20251486).

Supplementary Data

Training and testing datasets for machine learning models can be accessed online through the Mendeley Data: A Comprehensive Rubberized Concrete Dataset for Advanced Construction Practices (https://doi.org/10.17632/hpnrd55h4c.2).

Appendix

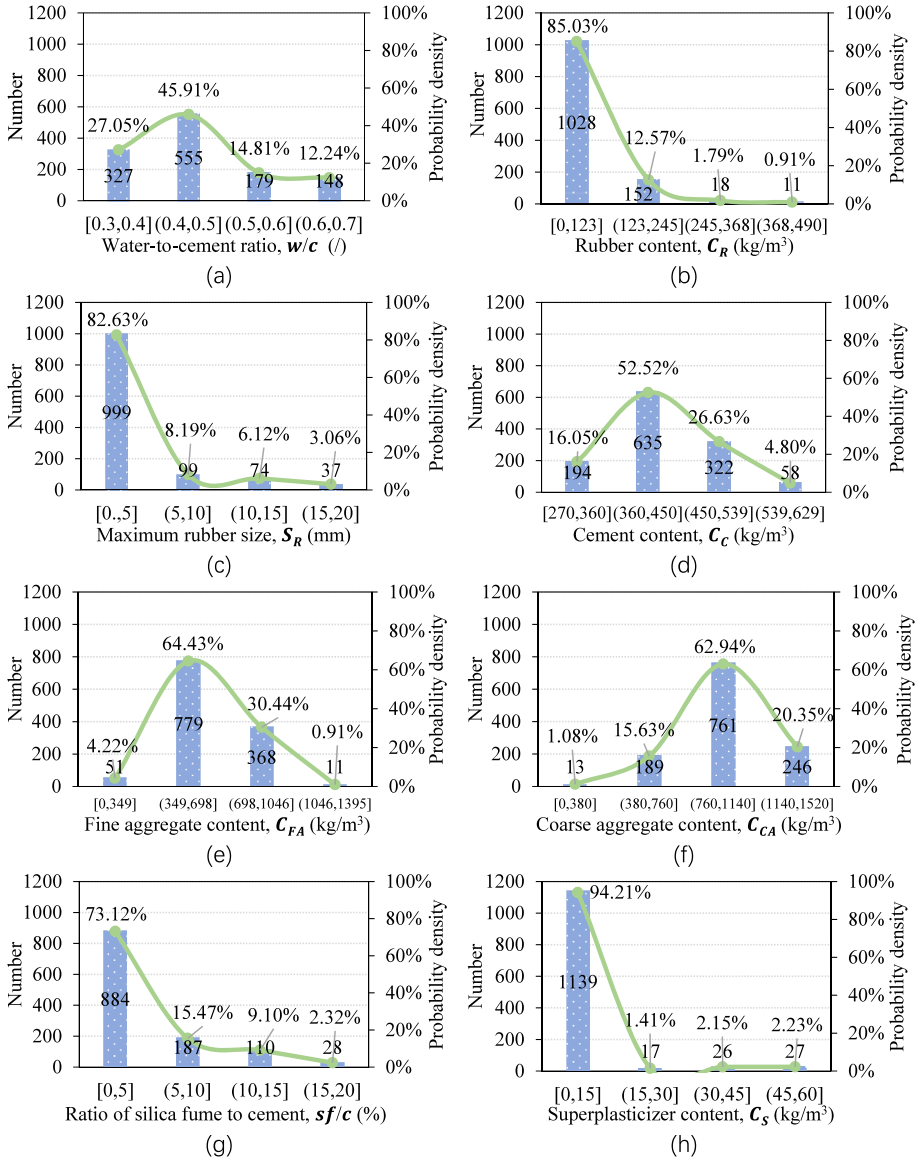

Fig. A1. Distribution of all input features and the compressive strength of rubberized concrete: (a) water-to-cement ratio; (b) rubber content; (c) maximum size of crumb rubber; (d) cement content; (e) fine aggregate contents; (f) coarse aggregate contents; (g) silica fume-to-cement ratio; (h) superplasticizer content; (i) curing time; and (j) compressive strength.

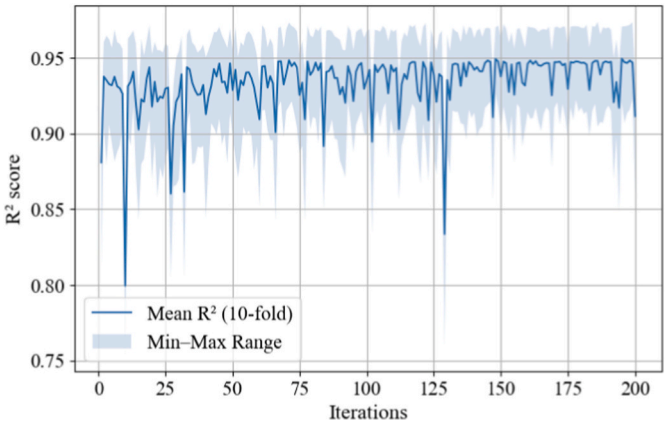

Fig. A2. R^2 across optimization iterations during Bayesian optimization of LightGBM. Bayesian optimization was performed with 10-fold CV, producing 10 validation results per iteration, from which the mean R^2 was calculated.

In Table A1, the "Type" column indicates the nature of each hyperparameter's value. Integer refers to whole-number parameters, such as tree depth or the number of estimators, where only discrete values are valid. For Integer types, the interval is typically set to 1, meaning the optimization process considers each integer within the range. Real denotes continuous numerical parameters that can take on any decimal value within a specified range. Some real-valued parameters are optimized on a logarithmic scale, noted as "Real (log)", which is useful for exploring values that span several orders of magnitude, such as learning rates or regularization strengths. Categorical parameters represent a fixed set of predefined options, such as loss functions or criteria, with no numerical relationship between the choices and are marked as N/A.

Table A1
Hyperparameter ranges for machine learning models

Models	Hyperparameter	Type	Min	Max	Interval
LightGBM	n_estimators	Integer	200	800	1
	max_depth	Integer	3	30	1
	learning_rate	Real (log)	0.01	0.5	Continuous
	reg_lambda	Real	0	10	1
	reg_alpha	Real	0	10	1
	num_leaves	Integer	20	100	1
	min_child_samples	Integer	1	100	1
SVM	C	Real (log)	1	1000	Continuous
	gamma	Real (log)	1	20	Continuous
	epsilon	Real	0.1	5	Continuous
RT	n_estimators	Integer	100	600	1
	max_depth	Integer	10	30	1
	max_leaf_nodes	Integer	100	600	1
	max_features	Integer	1	9	1
	criterion	Categorical	'squared_error', 'absolute_error', 'poisson'		N/A
ERT	n_estimators	Integer	100	500	1
	max_depth	Integer	5	20	1
	max_leaf_nodes	Integer	50	500	1
	criterion	Categorical	'friedman_mse', 'squared_error'		N/A
	max_features	Integer	1	9	1
XGBoost	n_estimators	Integer	200	800	1
	learning_rate	Real (log)	0.01	0.3	Continuous
	gamma	Real	0	3	Continuous
	max_depth	Integer	3	10	1
	reg_alpha	Real	0	5	Continuous
	reg_lambda	Real	0	10	Continuous
ANN	learning_rate_init	Real (log)	0.0001	0.1	Continuous
	Hidden_layer_size	Categorical	(50), (100), (150), (50, 100), (100, 150)		N/A
	alpha	Real (log)	0.0001	0.1	Continuous
	max_iter	Integer	1000	5000	1

Table A2
Optimal hyperparameters determined through Bayesian Optimization cross-validation

Algorithms	Hyperparameters	Descriptions
ANN	$n_{hl} = 2$	Number of the hidden layer
	$n_e = (153,140)$	Number of neurons in the 1st and 2nd hidden layer
	$l_r = 0.0003$	Learning rate
	$\alpha = 0.1$	Strength of the L2 regularization term
	max_iter = 2846	Maximum iterations

(*continued on next page*)

Table A2 (*continued*)

Algorithms	Hyperparameters	Descriptions
	Activation function: ReLu	ReLu function is used as the activation function
ERT	$n_e = 100$	Number of estimators
	$d_{\max} = 15$	Maximum depth of the tree
	$n_{\max} = 500$	Maximum number of leaf nodes
	$n_f = 9$	Limit number of features considered at each split
	Criterion: Squared error	Squared error is utilized to evaluate the splitting
SVM	$C = 343$	Control model complexity
	gamma = 10	Influences the scope of the kernel function
	epsilon = 1	Defines the tolerance range for errors
	kernel: rbf	rbf is adopted as the kernel function
RF	$n_e = 300$	Number of estimators
	$d_{\max} = 17$	Maximum depth of the tree
	$n_{\max} = 300$	Maximum number of leaf nodes
	$n_f = 7$	Limit number of features considered at each split
	Criterion: Poisson	Poisson is adopted as the splitting criterion
XGBoost	$n_e = 600$	Number of estimators
	$l_r = 0.16$	Learning rate
	$\gamma_0 = 0$	Minimum loss reduction for a further leaf partition
	$d_{\max} = 6$	Maximum depth of each tree
	reg_alpha = 5	L1 regularization term coefficient
	reg_lambda = 10	L2 regularization term coefficient
LightGBM	$n_e = 200$	Number of estimators
	$l_r = 0.29$	Learning rate
	$d_{\max} = 12$	Maximum depth of the tree
	$n = 20$	Number of leaves

Data availability

Data will be made available on request.

References

Abdullah, G.M., Chohan, I.M., Ali, M., Bheel, N., Ahmad, M., Najeh, T., Gamil, Y., Almujibah, H.R., 2024. Effect of titanium dioxide as nanomaterials on mechanical and durability properties of rubberised concrete by applying RSM modelling and optimizations. Front. Mater. 11, 1357094. https://doi.org/10.3389/fmats.2024.1357094.

Adegbemileke, S.A., Osuji, S.O., Ogirigbo, O.R., 2024. An assessment of the pozzolanic potential and mechanical properties of Nigerian calcined clays for sustainable ternary cement blends. Sustain. Struct. 4 (3), 1–15. https://doi.org/10.54113/j.sust.2024.000057.

Agrawal, D., Waghe, U., Ansari, K., Dighade, R., Amran, M., Qader, D.N., Fediuk, R., 2023. Experimental effect of pre-treatment of rubber fibers on mechanical properties of rubberized concrete. J. Mater. Res. Technol. 23, 791–807. https://doi.org/10.1016/j.jmrt.2023.01.027.

Agrawal, D., Waghe, U., Ansari, K., Amran, M., Gamil, Y., Alluqmani, A.E., Thakare, N., 2024. Optimization of eco-friendly concrete with recycled coarse aggregates and rubber particles as sustainable industrial byproducts for construction practices. Heliyon 10 (4), e25923. https://doi.org/10.1016/j.heliyon.2024.e25923.

Ahmad, A., Chaiyasarn, K., Farooq, F., Ahmad, W., Suparp, S., Aslam, F., 2021. Compressive strength prediction via gene expression programming (GEP) and artificial neural network (ANN) for concrete containing RCA. Buildings 11 (8), 324. https://doi.org/10.3390/buildings11080324.

Aiello, M.A., Leuzzi, F., 2010. Waste tyre rubberized concrete: properties at fresh and hardened state. Waste Manag. 30 (8–9), 1696–1704. https://doi.org/10.1016/j.wasman.2010.02.005.

Ali, R., Muayad, M., Mohammed, A.S., Asteris, P.G., 2023. Analysis and prediction of the effect of Nanosilica on the compressive strength of concrete with different mix proportions and specimen sizes using various numerical approaches. Struct. Concr. 24 (3), 4161–4184. https://doi-org.tudelft.idm.oclc.org/10.1002/suco.202200718.

Aliabdo, A.A., Abd Elmoaty, M., AbdElbaset, M.M., 2015. Utilization of waste rubber in non-structural applications. Constr. Build. Mater. 91, 195–207. https://doi.org/10.1016/j.conbuildmat.2015.05.080.

Alizadeh, M., Eftekhar, M.R., Asadi, P., Mostofinejad, D., 2024. Enhancing the mechanical properties of crumb rubber concrete through polypropylene mixing via a pre-mixing technique. Case Stud. Constr. Mater. 21, e03569. https://doi.org/10.1016/j.cscm.2024.e03569.

Alsalman, A., Dang, C.N., Martí-Vargas, J.R., Hale, W.M., 2020. Mixture-proportioning of economical UHPC mixtures. J. Build. Eng. 27, 100970. https://doi.org/10.1016/j.jobe.2019.100970.

Apicella, A., Donnarumma, F., Isgrò, F., Prevete, R., 2021. A survey on modern trainable activation functions. Neural Netw. 138, 14–32. https://doi.org/10.1016/j.neunet.2021.01.026.

Beiram, A.A., Al-Mutairee, H.M., 2022. The effect of chip rubber on the properties of concrete. Mater. Today Proc. 60, 1981–1988. https://doi.org/10.1016/j.matpr.2022.01.209.

Bergstra, J., Bengio, Y., 2012. Random search for hyper-parameter optimization. J. Mach. Learn. Res. 13 (1), 281–305. https://dl.acm.org/doi/abs/10.5555/2188385.2188395.

Bignozzi, M., Sandrolini, F., 2006. Tyre rubber waste recycling in self-compacting concrete. Cement Concr. Res. 36 (4), 735–739. https://doi.org/10.1016/j.cemconres.2005.12.011.

Bing, C., Ning, L., 2014. Experimental research on properties of fresh and hardened rubberized concrete. J. Mater. Civ. Eng. 26 (8), 04014040. https://doi.org/10.1061/(ASCE)MT.1943-5533.0000923.

Brieuc, M.S., Waters, C.D., Drinan, D.P., Naish, K.A., 2018. A practical introduction to Random Forest for genetic association studies in ecology and evolution. Mol. Ecol. Res. 18 (4), 755–766. https://doi.org/10.1111/1755-0998.12773.

Bulut, H., 2024. A different approach for green concrete production: determination of the effect of e-waste and waste rubber powder on durability properties of concrete. Challenge J. Concrete Res. Lett. 15 (3), 69–81. https://doi.org/10.20528/cjcrl.2024.03.001.

Che, Z., Purushotham, S., Khemani, R., Liu, Y., 2017. Interpretable deep models for ICU outcome prediction. In: AMIA Annual Symposium Proceedings. https://www.researchgate.net/publication/317085922.

Chen, T., Guestrin, C., 2016. Xgboost: a scalable tree boosting system. In: Proceedings of the 22nd ACM SIGKDD International Conference on Knowledge Discovery and Data Mining. https://dl.acm.org/doi/10.1145/2939672.2939785.

Chen, Z., Li, L., Xiong, Z., 2019. Investigation on the interfacial behaviour between the rubber-cement matrix of the rubberized concrete. J. Clean. Prod. 209, 1354–1364. https://doi.org/10.1016/j.jclepro.2018.10.305.

Chen, G., Zheng, D.-p., Chen, Y.-w., Lin, J.-X., Lao, W.-j., Guo, Y.-c., Chen, Z.-b., Lan, X.-w., 2023. Development of high performance geopolymer concrete with waste rubber and recycle steel fiber: a study on compressive behavior, carbon emissions and economical performance. Constr. Build. Mater. 393, 131988. https://doi.org/10.1016/j.conbuildmat.2023.131988.

Chiaia, B., Fantilli, A.P., Guerini, A., Volpatti, G., Zampini, D., 2014. Eco-mechanical index for structural concrete. Constr. Build. Mater. 67, 386–392. https://doi.org/10.1016/j.conbuildmat.2013.12.090.

Choudhary, S., Chaudhary, S., Jain, A., Gupta, R., 2020. Assessment of effect of rubber tyre fiber on functionally graded concrete. Mater. Today Proc. 28, 1496–1502. https://doi.org/10.1016/j.matpr.2020.04.830.

Chowdhurya, J.A., Islama, M.S., Islama, M.A., Al Bari, M.A., Debnatha, A.K., 2025. Analysis of mechanical properties of fly ash and boiler slag integrated geopolymer composites. Sustain. Struct. 5 (2), 000073. https://doi.org/10.54113/j.sust.2025.000073.

Cortes, C., Vapnik, V., 1995. Support-vector networks. Mach. Learn. 20 (3), 273–297. https://doi.org/10.1007/BF00994018.

Dai, J., Xiong, J.M., Zhou, J.Z., 2013. Experimental Study and analysis on strength properties of waste crumb rubber concrete. Adv. Mater. Res. 815, 227–232. https://doi.org/10.4028/www.scientific.net/AMR.815.227.

Dissanayake, D., Weerasinghe, D., Thebuwanage, L., Bandara, U., 2021. An environmentally friendly sound insulation material from post-industrial textile waste

and natural rubber. J. Build. Eng. 33, 101606. https://doi.org/10.1016/j.jobe.2020.101606.
Ejaz, U., Khan, S.M., Jehangir, S., Ahmad, Z., Abdullah, A., Iqbal, M., Khalid, N., Nazir, A., Svenning, J.-C., 2024. Monitoring the industrial waste polluted stream-integrated analytics and machine learning for water quality index assessment. J. Clean. Prod. 450, 141877. https://doi.org/10.1016/j.jclepro.2024.141877.
El-Gammal, A., Abdel-Gawad, A., El-Sherbini, Y., Shalaby, A., 2010. Compressive strength of concrete utilizing waste tire rubber. J. Emerg. Trends Eng. Appl. Sci. 1 (1), 96–99. DOI. http://hdl.handle.net/10520/EJC156734.
Elbialy, S., Ibrahim, W., Mahmoud, S., Ayash, N.M., Mamdouh, H., 2024. Mechanical characteristics and structural performance of rubberized concrete: experimental and analytical analysis. Case Stud. Constr. Mater. 21, e03727. https://doi.org/10.1016/j.cscm.2024.e03727.
Fadiel, A.A., Mohammed, N.S., Abu-Lebdeh, T., Munteanu, I.S., Niculae, E., Petrescu, F.I. T., 2023a. A comprehensive evaluation of the mechanical properties of rubberized concrete. J. Compos. Sci. 7 (3), 129. https://doi.org/10.3390/jcs7030129.
Fadiel, A.A., Abu-Lebdeh, T., Munteanu, I.S., Niculae, E., Petrescu, F.I.T., 2023b. Mechanical properties of rubberized concrete at elevated temperatures. J. Compos. Sci. 7 (7), 283. https://doi.org/10.3390/jcs7070283.
Faraj, R.H., Sherwani, A.F.H., Daraei, A., 2019. Mechanical, fracture and durability properties of self-compacting high strength concrete containing recycled polypropylene plastic particles. J. Build. Eng. 25, 100808. https://doi.org/10.1016/j.jobe.2019.100808.
Fernández-Ruiz, M.A., Gil-Martín, L.M., Carbonell-Márquez, J.F., Hernández-Montes, E., 2018. Epoxy resin and ground tyre rubber replacement for cement in concrete: compressive behaviour and durability properties. Constr. Build. Mater. 173, 49–57. https://doi.org/10.1016/j.conbuildmat.2018.04.004.
Gardner, W.A., 1984. Learning characteristics of stochastic-gradient-descent algorithms: a general study, analysis, and critique. Signal Process. 6 (2), 113–133. https://doi.org/10.1016/0165-1684(84)90013-6.
Gesoğlu, M., Güneyisi, E., 2007. Strength development and chloride penetration in rubberized concretes with and without silica fume. Mater. Struct. 40 (9), 953–964. https://doi.org/10.1617/s11527-007-9279-0.
Gesoglu, M., Güneyisi, E., Hansu, O., İpek, S., Asaad, D.S., 2015. Influence of waste rubber utilization on the fracture and steel–concrete bond strength properties of concrete. Constr. Build. Mater. 101, 1113–1121. https://doi.org/10.1016/j.conbuildmat.2015.10.030.
Geurts, P., Ernst, D., Wehenkel, L., 2006. Extremely randomized trees. Mach. Learn. 63 (1), 3–42. https://doi.org/10.1007/s10994-006-6226-1.
Gregori, A., Castoro, C., Venkiteela, G., 2021. Predicting the compressive strength of rubberized concrete using artificial intelligence methods. Sustainability 13 (14), 7729. https://doi.org/10.3390/su13147729.
Güneyisi, E., 2010. Fresh properties of self-compacting rubberized concrete incorporated with fly ash. Mater. Struct. 43 (8), 1037–1048. https://doi.org/10.1617/s11527-009-9564-1.
Güneyisi, E., Gesoğlu, M., Özturan, T., 2004. Properties of rubberized concretes containing silica fume. Cement Concr. Res. 34 (12), 2309–2317. https://doi.org/10.1016/j.cemconres.2004.04.005.
Guo, S., Dai, Q., Si, R., Sun, X., Lu, C., 2017. Evaluation of properties and performance of rubber-modified concrete for recycling of waste scrap tire. J. Clean. Prod. 148, 681–689. https://doi.org/10.1016/j.jclepro.2017.02.046.
Guo, P., Meng, W., Xu, M., Li, V.C., Bao, Y., 2021. Predicting mechanical properties of high-performance fiber-reinforced cementitious composites by integrating micromechanics and machine learning. Materials 14 (12), 3143. https://doi.org/10.3390/ma14123143.
Guo, P., Mahjoubi, S., Liu, K., Meng, W., Bao, Y., 2023a. Self-updatable AI-assisted design of low-carbon cost-effective ultra-high-performance concrete (UHPC). Case Stud. Constr. Mater. 19, e02625. https://doi.org/10.1016/j.cscm.2023.e02625.
Guo, P., Meng, W., Du, J., Stevenson, L., Han, B., Bao, Y., 2023b. Lightweight ultra-high-performance concrete (UHPC) with expanded glass aggregate: development, characterization, and life-cycle assessment. Constr. Build. Mater. 371, 130441. https://doi.org/10.1016/j.conbuildmat.2023.130441.
Guo, P., Meng, W., Bao, Y., 2024. Knowledge-guided data-driven design of ultra-high-performance geopolymer (UHPG). Cement Concr. Compos. 153, 105723. https://doi.org/10.1016/j.cemconcomp.2024.105723.
Guo, P., Moghaddas, S.A., Liu, Y., Meng, W., Li, V.C., Bao, Y., 2025. Applications of machine learning methods for design and characterization of high-performance fiber-reinforced cementitious composite (HPFRCC): a review. J. Sustain. Cement-Based Mater. 1–24. https://doi.org/10.1080/21650373.2025.2462183.
Gupta, T., Chaudhary, S., Sharma, R.K., 2016. Mechanical and durability properties of waste rubber fiber concrete with and without silica fume. J. Clean. Prod. 112, 702–711. https://doi.org/10.1016/j.jclepro.2015.07.081.
Gupta, T., Siddique, S., Sharma, R.K., Chaudhary, S., 2021a. Investigating mechanical properties and durability of concrete containing recycled rubber ash and fibers. J. Mater. Cycles Waste Manag. 23 (3), 1048–1057. https://doi.org/10.1007/s10163-021-01192-w.
Gupta, T., Siddique, S., Sharma, R.K., Chaudhary, S., 2021b. Effect of aggressive environment on durability of concrete containing fibrous rubber shreds and silica fume. Struct. Concr. 22 (5), 2611–2623. https://doi.org/10.1002/suco.202000043.
Jaf, D.K.I., Abdalla, A., Mohammed, A.S., Abdulrahman, P.I., Kurda, R., Mohammed, A. A., 2024. Hybrid nonlinear regression model versus MARS, MEP, and ANN to evaluate the effect of the size and content of waste tire rubber on the compressive strength of concrete. Heliyon 10 (4), e25997. https://doi.org/10.1016/j.heliyon.2024.e25997.
Jain, A., Nandakumar, K., Ross, A., 2005. Score normalization in multimodal biometric systems. Pattern Recogn. 38 (12), 2270–2285. https://doi.org/10.1016/j.patcog.2005.01.012.
Jalal, M., Nassir, N., Jalal, H., 2019. Waste tire rubber and pozzolans in concrete: a trade-off between cleaner production and mechanical properties in a greener concrete. J. Clean. Prod. 238, 117882. https://doi.org/10.1016/j.jclepro.2019.117882.
Karunarathna, S., Ngo, T., Linforth, S., Kashani, A., Liu, X., Lu, G., Ruan, D., 2022. Evaluation of the effect of recycled rubber aggregate size on concrete for sustainable applications of rubberised concrete in impact resistant structures: experimental and numerical study. J. Clean. Prod. 374, 133648. https://doi.org/10.1016/j.jclepro.2022.133648.
Kashem, A., Karim, R., Malo, S.C., Das, P., Datta, S.D., Alharthai, M., 2024. Hybrid data-driven approaches to predicting the compressive strength of ultra-high-performance concrete using SHAP and PDP analyses. Case Stud. Constr. Mater. 20, e02991. https://doi.org/10.1016/j.cscm.2024.e02991.
Kaveh, A., 2024. Applications of Artificial Neural Networks and Machine Learning in Civil Engineering, vol 1168. Springer.
Ke, G., Meng, Q., Finley, T., Wang, T., Chen, W., Ma, W., Ye, Q., Liu, T.-Y., 2017. Lightgbm: a highly efficient gradient boosting decision tree. In: Proceedings of the 31st International Conference on Neural Information Processing Systems. neurips, proceedings, pp. 3149–3157 cc/paper/2017/file/6449f44a102fde848669bdd9eb6b76fa-Paper.pdf.
Kechkar, C., Belachia, M., Cherait, Y., 2020. Contribution to the study of the durability of rubberized concrete in aggressive environments. Civ. Environ. Eng. Rep. 30 (1), 111–129. https://doi.org/10.2478/ceer-2020-0009.
Kelechi, S.E., Adamu, M., Mohammed, A., Ibrahim, Y.E., Obianyo, I.I., 2022. Durability performance of self-compacting concrete containing crumb rubber, fly ash and calcium carbide waste. Materials 15 (2), 488. https://doi.org/10.3390/ma15020488.
Khan, M., McNally, C., 2023. A holistic review on the contribution of civil engineers for driving sustainable concrete construction in the built environment. Dev. Built Environ. 16, 100273. https://doi.org/10.1016/j.dibe.2023.100273.
Khan, M., Lao, J., Dai, J.-G., 2022. Comparative study of advanced computational techniques for estimating the compressive strength of UHPC. J. Asian Concrete Feder. 8 (1), 51–68. https://doi.org/10.18702/acf.2022.6.8.1.51.
Khern, Y.C., Paul, S.C., Kong, S.Y., Babafemi, A.J., Anggraini, V., Miah, M.J., Šavija, B., 2020. Impact of chemically treated waste rubber tire aggregates on mechanical, durability and thermal properties of concrete. Front. Mater. 7, 90. https://doi.org/10.3389/fmats.2020.00090.
Kovačević, M., Lozančić, S., Nyarko, E.K., Hadzima-Nyarko, M., 2021. Modeling of compressive strength of self-compacting rubberized concrete using machine learning. Materials 14 (15), 4346. https://doi.org/10.3390/ma14154346.
Kumar, R., Dev, N., Ram, S., Verma, M., 2023. Investigation of dry-wet cycles effect on the durability of modified rubberised concrete. Force. Mech. 10, 100168. https://doi.org/10.1016/j.finmec.2023.100168.
Lavagna, L., Nisticò, R., Sarasso, M., Pavese, M., 2020. An analytical mini-review on the compression strength of rubberized concrete as a function of the amount of recycled tires crumb rubber. Materials 13 (5), 1234. https://doi.org/10.3390/ma13051234.
Lee, J.A., Sagong, M.J., Jung, J., Kim, E.S., Kim, H.S., 2023. Explainable machine learning for understanding and predicting geometry and defect types in Fe-Ni alloys fabricated by laser metal deposition additive manufacturing. J. Mater. Res. Technol. 22, 413–423. https://doi.org/10.1016/j.jmrt.2022.11.137.
Li, G., Wang, Z., Leung, C.K., Tang, S., Pan, J., Huang, W., Chen, E., 2016a. Properties of rubberized concrete modified by using silane coupling agent and carboxylated SBR. J. Clean. Prod. 112, 797–807. https://doi.org/10.1016/j.jclepro.2015.06.099.
Li, G., Wang, Z., Leung, C.K., Tang, S., Pan, J., Huang, W., Chen, E., 2016b. Properties of rubberized concrete modified by using silane coupling agent and carboxylated SBR. J. Clean. Prod. 112, 797–807. https://doi.org/10.1016/j.jclepro.2015.06.099.
Liu, F., Zheng, W., Li, L., Feng, W., Ning, G., 2013. Mechanical and fatigue performance of rubber concrete. Constr. Build. Mater. 47, 711–719. https://doi.org/10.1016/j.conbuildmat.2013.05.055.
Liu, H., Wang, X., Jiao, Y., Sha, T., 2016. Experimental investigation of the mechanical and durability properties of crumb rubber concrete. Materials 9 (3), 172. https://doi.org/10.3390/ma9030172.
Liu, Y., He, C., Huang, J., Xiao, X., Huang, W., Zhou, Z., 2020. Influence of rubber aggregate equal volume to replace fine aggregate on compressive strength of concrete. Bull. Chinese Ceram. Soc. 39 (9), 2807–2814. https://doi.org/10.16552/j.cnki.issn1001-1625.2020.09.014.
Luong, N.D., Long, H.V., Tuan, N.K., Thai, N.D., 2017. Properties of concrete containing rubber aggregate derived from discarded tires. Asian Rev. Environ. Earth Sci. 4 (1), 12–19. https://doi.org/10.20448/journal.506.2017.41.12.19.
Lv, J., Du, Q., Zhou, T., He, Z., Li, K., 2019. Fresh and mechanical properties of self-compacting rubber lightweight aggregate concrete and corresponding mortar. Adv. Mater. Sci. Eng. 2019 (1), 8372547. https://doi.org/10.1155/2019/8372547.
Ly, H.-B., Nguyen, T.-A., Tran, V.Q., 2021. Development of deep neural network model to predict the compressive strength of rubber concrete. Constr. Build. Mater. 301, 124081. https://doi.org/10.1016/j.conbuildmat.2021.124081.
Ma, Q.W., Yue, J.C., 2013. Effect on mechanical properties of rubberized concrete due to pretreatment of waste tire rubber with NaOH. Appl. Mech. Mater. 357, 897–904. https://doi.org/10.4028/www.scientific.net/AMR.815.227.
Mahjoubi, S., Barhemat, R., Guo, P., Meng, W., Bao, Y., 2021. Prediction and multi-objective optimization of mechanical, economical, and environmental properties for strain-hardening cementitious composites (SHCC) based on automated machine learning and metaheuristic algorithms. J. Clean. Prod. 329, 129665. https://doi.org/10.1016/j.jclepro.2021.129665.

Mahjoubi, S., Barhemat, R., Meng, W., Bao, Y., 2025. Review of AI-assisted design of low-carbon cost-effective concrete toward carbon neutrality. Artif. Intell. Rev. 58 (8), 225. https://doi.org/10.1007/s10462-025-11182-1.
Mansur, M., Islam, M., 2002. Interpretation of concrete strength for nonstandard specimens. J. Mater. Civ. Eng. 14 (2), 151–155. https://doi.org/10.1061/(ASCE)0899-1561(2002)14:2(151).
Maurya, K.K., Rawat, A., Shanker, R., 2023. Performance evaluation concept for crack healing in bacterial concrete structure using electro mechanical impedance technique with PZT patch. Dev. Built Environ. 15, 100196. https://doi.org/10.1016/j.dibe.2023.100196.
Medina, N.F., Flores-Medina, D., Hernández-Olivares, F., 2016. Influence of fibers partially coated with rubber from tire recycling as aggregate on the acoustical properties of rubberized concrete. Constr. Build. Mater. 129, 25–36. https://doi.org/10.1016/j.conbuildmat.2016.11.007.
Mehdipour, S., Nikbin, I.M., Dezhampanah, S., Mohebbi, R., Moghadam, H., Charkhtab, S., Moradi, A., 2020. Mechanical properties, durability and environmental evaluation of rubberized concrete incorporating steel fiber and metakaolin at elevated temperatures. J. Clean. Prod. 254, 120126. https://doi.org/10.1016/j.jclepro.2020.120126.
Mishra, M., Panda, K., 2015. An experimental study on fresh and hardened properties of self compacting rubberized concrete. Indian J. Sci. Technol. 8 (29), 1–8. https://doi.org/10.17485/ijst/2015/v8i29/86799.
Mohammed, B.S., Azmi, N., 2014. Strength reduction factors for structural rubbercrete. Front. Struct. Civ. Eng. 8 (3), 270–281. https://doi.org/10.1007/s11709-014-0265-7.
Mohd Nasir, N.A., Abu Bakar, N., Safiee, N.A., Abdul Aziz, F.N.A., 2022. Permeation-durability properties of metakaolin blended concrete containing rubber. Europ. J. Environ. Civil Eng. 26 (11), 5113–5128. https://doi.org/10.1080/19648189.2021.1885499.
Moolchandani, K., Sharma, A., Kishan, D., 2024. Enhancing concrete performance with crumb rubber and waste materials: a study on mechanical and durability properties. Buildings 14 (1), 161. https://doi.org/10.3390/buildings14010161.
Moustafa, A., Gheni, A., ElGawady, M.A., 2017. Shaking-table testing of high energy–dissipating rubberized concrete columns. J. Bridge Eng. 22 (8), 04017042. https://doi.org/10.1061/(ASCE)BE.1943-5592.0001077.
Neville, A.M., 1995. Propertie. Concr. 4. https://books.google.co.uk/books/about/Properties_of_concrete.html?id=mKEeAQAAIAAJ&redir_esc=y.
Ngu, J.C.Y., Yeo, W.S., Thien, T.F., Nandong, J., 2024. A comprehensive overview of the applications of kernel functions and data-driven models in regression and classification tasks in the context of software sensors. Appl. Soft Comput. 164, 111975. https://doi.org/10.1016/j.asoc.2024.111975.
Noaman, A.T., Bakar, B.A., Akil, H.M., Alani, A., 2017. Fracture characteristics of plain and steel fibre reinforced rubberized concrete. Constr. Build. Mater. 152, 414–423. https://doi.org/10.1016/j.conbuildmat.2017.06.127.
Paruthi, S., Husain, A., Alam, P., Khan, A.H., Hasan, M.A., Magbool, H.M., 2022. A review on material mix proportion and strength influence parameters of geopolymer concrete: application of ANN model for GPC strength prediction. Constr. Build. Mater. 356, 129253. https://doi.org/10.1016/j.conbuildmat.2022.129253.
Pham, T.M., Zhang, X., Elchalakani, M., Karrech, A., Hao, H., Ryan, A., 2018. Dynamic response of rubberized concrete columns with and without FRP confinement subjected to lateral impact. Constr. Build. Mater. 186, 207–218. https://doi.org/10.1016/j.conbuildmat.2018.07.146.
Pham, T.M., Elchalakani, M., Hao, H., Lai, J., Ameduri, S., Tran, T.M., 2019. Durability characteristics of lightweight rubberized concrete. Constr. Build. Mater. 224, 584–599. https://doi.org/10.1016/j.conbuildmat.2019.07.048.
Prasad, A.M., Iverson, L.R., Liaw, A., 2006. Newer classification and regression tree techniques: bagging and random forests for ecological prediction. Ecosystems 9 (2), 181–199. https://doi.org/10.1007/s10021-005-0054-1.
Rahat Dahmardeh, S., Sargazi Moghaddam, M.S., Mirabi Moghaddam, M.H., 2021. Effects of waste glass and rubber on the SCC: rheological, mechanical, and durability properties. Europ. J. Environ. Civil Eng. 25 (2), 302–321. https://doi.org/10.1080/19648189.2018.1528891.
Rezaifar, O., Hasanzadeh, M., Gholhaki, M., 2016. Concrete made with hybrid blends of crumb rubber and metakaolin: optimization using Response Surface Method. Constr. Build. Mater. 123, 59–68. https://doi.org/10.1016/j.conbuildmat.2016.06.047.
Safan, M., Eid, F.M., Awad, M., 2017. Enhanced properties of crumb rubber and its application in rubberized concrete. Int. J. Curr. Eng. Technol. 7 (5), 1784–1790. DOI: inpressco.com/wp-content/uploads/2017/09/Paper161784-1790.pdf.
Saini, R., Chaturvedy, G.K., Pandey, U.K., 2024. Examining the effects of nano iron oxide on physical and mechanical characteristics of rubberized concrete. Innovative Infrastruct. Solution. 9 (6), 180. https://doi.org/10.1007/s41062-024-01494-6.
Sanjaya, B., Mohamed, A., Appuhamy, J., Bandara, W., Venkatesan, S., Gravina, R., 2023. Properties of rubberized concrete at low-level replacement ratio with smaller rubber particle: an experimental investigation. In: In Proceedings of the 9th International Symposium on Advances in Civil and Environmental Engineering Practices for Sustainable Development. www.researchgate.net/publication/371450091.
Sathiparan, N., Subramaniam, D.N., 2025. Optimizing fly ash and rice husk ash as cement replacements on the mechanical characteristics of pervious concrete. Sustain. Struct. 5. https://doi.org/10.54113/j.sust.2025.000065.
Sharma, J., Chaturvedi, G.K., Pandey, U.K., 2024. Impact of Nano Titanium Dioxide on Rubberized Concrete: Evaluating Physical, Mechanical, and Durability Characteristics. https://doi.org/10.2139/ssrn.5072487. Available at: SSRN.
Sherwani, A.F.H., Abdulrahman, P.I., Younis, K.H., Mohammed, A.S., Zrar, Y.J., 2025. Compressive strength modeling of the eco-friendly self-compacting rubberized concrete with fly ash and ground granulated blast furnace slag additives. Innovative Infrastruct. Solution. 10 (2), 61. https://doi.org/10.1007/s41062-024-01811-z.
Singh, D., Singh, B., 2020. Investigating the impact of data normalization on classification performance. Appl. Soft Comput. 97, 105524. https://doi.org/10.1016/j.asoc.2019.105524.
Singh, G., Tiwary, A.K., Singh, S., Kumar, R., Chohan, J.S., Sharma, S., Li, C., Sharma, P., Deifalla, A.F., 2022. Incorporation of silica fumes and waste glass powder on concrete properties containing crumb rubber as a partial replacement of fine aggregates. Sustainability 14 (21), 14453. https://doi.org/10.3390/su142114453.
Sinkhonde, D., 2023. Modeling and experimental studies on energy consumption and properties of concrete containing waste brick powder and waste tire rubber for sustainable construction. Clean. Eng. Technol. 13, 100631. https://doi.org/10.1016/j.clet.2023.100631.
Skripkiūnas, G., Grinys, A., Miškinis, K., 2009. Damping properties of concrete with rubber waste additives. Mater. Sci. 15 (3), 266–272. www.matsc.ktu.lt/index.php/MatSc/article/view/26160.
Strukar, K., Kalman Šipoš, T., Dokšanović, T., Rodrigues, H., 2018. Experimental study of rubberized concrete stress-strain behavior for improving constitutive models. Materials 11 (11), 2245. https://doi.org/10.3390/ma11112245.
Sun, Y., Ding, S., Zhang, Z., Jia, W., 2021a. An improved grid search algorithm to optimize SVR for prediction. Soft Comput. 25 (7), 5633–5644. https://doi.org/10.1007/s00500-020-05560-w.
Sun, X., Zhao, Y., Tian, Y., Wu, P., Guo, Z., Qiu, J., Xing, J., Xiaowei, G., 2021b. Modification of high-volume fly ash cement with metakaolin for its utilization in cemented paste backfill: the effects of metakaolin content and particle size. Powder Technol. 393, 539–549. https://doi.org/10.1016/j.powtec.2021.07.067.
Surehali, S., Singh, A., Biligiri, K.P., 2023. A state-of-the-art review on recycling rubber in concrete: sustainability aspects, specialty mixtures, and treatment methods. Dev. Built Environ. 14, 100171. https://doi.org/10.1016/j.dibe.2023.100171.
Thomas, B.S., Gupta, R.C., 2016a. Properties of high strength concrete containing scrap tire rubber. J. Clean. Prod. 113, 86–92. https://doi.org/10.1016/j.jclepro.2015.11.019.
Thomas, B.S., Gupta, R.C., 2016b. A comprehensive review on the applications of waste tire rubber in cement concrete. Renew. Sustain. Energy Rev. 54, 1323–1333. https://doi.org/10.1016/j.rser.2015.10.092.
Thomas, B.S., Gupta, R.C., Kalla, P., Cseteneyi, L., 2014. Strength, abrasion and permeation characteristics of cement concrete containing discarded rubber fine aggregates. Constr. Build. Mater. 59, 204–212. https://doi.org/10.1016/j.conbuildmat.2014.01.074.
Topcu, I.B., 1995. The properties of rubberized concretes. Cement Concr. Res. 25 (2), 304–310. https://doi.org/10.1016/0008-8846(95)00014-3.
Topçu, İ.B., Bilir, T., 2009. Experimental investigation of some fresh and hardened properties of rubberized self-compacting concrete. Mater. Des. 30 (8), 3056–3065. https://doi.org/10.1016/j.matdes.2008.12.011.
Wu, J., Chen, X.-Y., Zhang, H., Xiong, L.-D., Lei, H., Deng, S.-H., 2019. Hyperparameter optimization for machine learning models based on Bayesian optimization. J. Electron. Sci. Technol. 17 (1), 26–40. https://doi.org/10.11989/JEST.1674-862X.80904120.
Xie, Y., Ebad Sichani, M., Padgett, J.E., DesRoches, R., 2020. The promise of implementing machine learning in earthquake engineering: a state-of-the-art review. Earthq. Spectra 36 (4), 1769–1801. https://doi.org/10.1177/8755293020919419.
Xue, G., Sun, L., Wan, Z., 2022. Study on compressive strength of rubber concrete cube based on meso-level. Concrete 387, 84–87. https://doi.org/10.3969/j.issn.1002-3550.2022.01.019.
Yasser, N., Abdelrahman, A., Kohail, M., Moustafa, A., 2023. Experimental investigation of durability properties of rubberized concrete. Ain Shams Eng. J. 14 (6), 102111. https://doi.org/10.1016/j.asej.2022.102111.
Youssf, O., Mills, J.E., Hassanli, R., 2016. Assessment of the mechanical performance of crumb rubber concrete. Constr. Build. Mater. 125, 175–183. https://doi.org/10.1016/j.conbuildmat.2016.08.040.
Záleská, M., Pavlík, Z., Čítek, D., Jankovský, O., Pavlíková, M., 2019. Eco-friendly concrete with scrap-tyre-rubber-based aggregate–Properties and thermal stability. Constr. Build. Mater. 225, 709–722. https://doi.org/10.1016/j.conbuildmat.2019.07.168.
Zhang, B., Poon, C.S., 2018. Sound insulation properties of rubberized lightweight aggregate concrete. J. Clean. Prod. 172, 3176–3185. https://doi.org/10.1016/j.jclepro.2017.11.044.
Zhang, H., Gou, M., Liu, X., Guan, X., 2014. Effect of rubber particle modification on properties of rubberized concrete. J. Wuhan Univ. Technol.-Materials Sci. Ed. 29 (4), 763–768. https://doi.org/10.1007/s11595-014-0993-5.
Zhang, Y., Aslani, F., Lehane, B., 2021. Compressive strength of rubberized concrete: regression and GA-BPNN approaches using ultrasonic pulse velocity. Constr. Build. Mater. 307, 124951. https://doi.org/10.1016/j.conbuildmat.2021.124951.
Zhang, W., Liu, D., Cao, K., 2024. Prediction of concrete compressive strength using support vector machine regression and non-destructive testing. Case Stud. Constr. Mater. 21, e03416. https://doi.org/10.1016/j.cscm.2024.e03416.
Zhou, C., Zheng, Y., 2025. Data-driven compressive strength investigation and design suggestions for rubberized concrete. Mater. Today Commun. 46, 112477. https://doi.org/10.1016/j.mtcomm.2025.112477.
Zhou, C., Wang, W., Zheng, Y., Liu, X., Cao, H., Hui, Y., 2023. Dynamic behavior of RC columns confined with CFRP grid-reinforced ECC subjected to lateral low-velocity impact. Int. J. Impact Eng. 172, 104402. https://doi.org/10.1016/j.ijimpeng.2022.104402.
Zhou, C., Wang, W., Zheng, Y., 2024. Data-driven shear capacity analysis of headed stud in steel-UHPC composite structures. Eng. Struct. 321, 118946. https://doi.org/10.1016/j.engstruct.2024.118946.

Zhou, C., Tan, X., Zheng, Y., Wang, Y., Mahjoubi, S., 2025. Data-driven axial bearing capacity analysis of steel tubes infilled with rubberized alkali-activated concrete. Adv. Struct. Eng. 28 (1), 145–158. https://doi.org/10.1177/13694332241268243.
Zhu, X., Jiang, Z., 2023. Reuse of waste rubber in pervious concrete: experiment and DEM simulation. J. Build. Eng. 71, 106452. https://doi.org/10.1016/j.jobe.2023.106452.
Zinkaah, O.H., Alridha, Z., Alhawat, M., Khan, A., 2024. Mechanical and thermal properties of rubberized concrete incorporated silica fume. Muthanna J. Eng. Technol. 12 (1). https://doi.org/10.52113/3/eng/mjet/2024-12-01/63-71.
Zrar, Y.J., Abdulrahman, P.I., Sherwani, A.F.H., Younis, K.H., Mohammed, A.S., 2024. Sustainable innovation in self-compacted concrete: integrating by-products and waste rubber for green construction practices. Structures 62, 106234. https://doi.org/10.1016/j.istruc.2024.106234.